GABA and glycine in retinal amacrine cells: combined Golgi impregnation and immunocytochemistry

DAVID M. SHERRY* AND STEPHEN YAZULLA

Department of Neurobiology and Behavior, State University of New York at Stony Brook, Stony Brook, New York 11794-5230, U.S.A.

CONTENTS

SUMMARY

Golgi-impregnated amacrine cells in the all-cone lizard retina (*Anolis carolinensis*) were characterized on the bases of dendritic and somatic criteria. Four major cell categories, comprising 23 types were identified: three non-stratified, 13 monostratified, five bistratified, and two tristratified types. Four of the cell types comprised two to four subtypes based on stratification of their dendrites within the inner plexiform layer (IPL). Golgi impregnation strongly favoured monostratified amacrine cells with cell bodies at the proximal margin of the inner nuclear layer.

The neurotransmitter content of each of the 23 amacrine cell types was examined by combined Golgi–immunocytochemistry after morphological classification. Putative neurotransmitters examined included gamma-aminobutyric acid (GABA), glycine (GLY) and aspartate (ASP). Seventeen cell types showed GABA-immunoreactivity (IR), three cell types showed GLY-IR, and four cell types showed neither GABA-IR nor GLY-IR. No cell types showed ASP-IR. Each cell type had a characteristic neurochemical signature, with the exception of one monostratified cell type that showed three different neurochemical signatures.

Postembedding immunocytochemistry on conventionally processed retinas confirmed the localization of glutamic acid decarboxylase, the synthetic enzyme for GABA, to cells similar to several of the GABA-IR Golgi-stained types. Postembedding immunocytochemistry for tyrosine hydroxylase (the synthetic

* Present Address and corresponding author: Department of Physiology and Biophysics, Room C-552, Cornell University Medical College, 1300 York Avenue, New York, New York 10021, U.S.A.

Phil. Trans. R. Soc. Lond. B (1993) **342**, 295–320
Printed in Great Britain

enzyme for catecholamines) and GABA on serial sections demonstrated colocalization of GABA and a catecholamine, probably dopamine, in a bistratified amacrine cell type.

We conclude that GABA-IR amacrine cell types are more numerous and morphologically heterogeneous than GLY-IR amacrine cells. The morphological heterogeneity and, with one exception, exclusivity of GABA-IR and GLY-IR amacrine cell types indicate that both neurotransmitters play a variety and different functional roles in the lizard inner retina.

1. INTRODUCTION

Retinal amacrine cells are a highly heterogeneous class of interneuron that mediate lateral interactions in the inner plexiform layer (IPL) through complex synaptic interactions with bipolar, ganglion, and other amacrine cells (Dowling & Boycott 1966; Dowling 1968; Masland 1988). Amacrine cells comprise a wide variety of morphological (cf. Ramon y Cajal 1933; Kolb 1982; Wagner & Wagner 1988), neurochemical (see review by Brecha 1983) and physiological types (cf. Famiglietti *et al.* 1977; Teranishi *et al.* 1987; Ammermüller & Weiler 1989), but many questions about the functional organization of amacrine cells remain.

A large number of classical and peptide neurotransmitter substances have been localized to amacrine cells (Brecha 1983), but most amacrine cells appear to employ an inhibitory amino acid neurotransmitter, either gamma-aminobutyric acid (GABA) or glycine (GLY). GABA and GLY each are found in about 30–40% of all amacrine cells, and both substances are found in multiple amacrine cell types (see reviews by Marc 1985; Yazulla 1986). Amacrine cell populations that contain GABA and GLY are very distinct. GABA and GLY colocalize in about 5% of all GLY-containing amacrine cells in the retinas of several species, including tiger salamander, cat, human and lizard (Yang & Yazulla 1988; Pourcho & Owczarzak 1991; Davanger *et al.* 1991; Sherry *et al.* 1993) but do not colocalize in goldfish retina (Yazulla & Studholme 1990). The number and variety of GABA- and GLY-containing amacrine cells and the complexity of GLY and GABA circuitry in the IPL have hampered the determination of the number and the morphology of individual GABA- or GLY-containing cell types and their contributions to retinal circuitry.

The retinas of diurnal lizards contain only cone photoreceptors (reviewed by Crescitelli 1972) and offer an excellent opportunity to study amacrine cells that subserve cone pathways. The lizard *Anolis carolinensis* is a diurnal visual predator possessing color vision (Hodgekinson & Still 1980) that is probably mediated by three visual pigments (Provencio *et al.* 1992). The retina of this species has a deep convexiclivate central fovea and parafovea, defined by the convoluted region of the outer plexiform layer (OPL) (Makaretz & Levine 1980). This species also has a simple, two dimensional cone mosaic (Underwood 1951), and some basic anatomical and neurochemical features of *Anolis* amacrine cells are known. For example, *Anolis* amacrine cells that contain GABA tend to have larger processes and larger, more proximally placed somas in the inner nuclear layer (INL) than GLY-containing amacrine cells; both GABA- and GLY-containing amacrine cells comprise multiple types, and an amacrine cell type that colocalizes GABA and GLY has been identified (Sherry & Ulshafer 1992*a*; Sherry *et al.* 1993). Two types of amacrine cells that contain aspartate (ASP) also have been described (Sherry & Ulshafer 1992*b*).

We examined the anatomical and neurochemical diversity of amacrine cells in the *Anolis* retina using a combined Golgi–immunocytochemistry technique. This approach revealed a great diversity of GABA- and GLY-containing amacrine cell types and complex dendritic organization in the IPL.

2. MATERIALS AND METHODS

(*a*) *Animal maintenance*

Adult lizards (*Anolis carolinensis*) were maintained in a light box on a 12 h light:12 h dark cycle for several weeks prior to use. Crickets and water were available at all times.

(*b*) *Golgi processing and thick sectioning*

Golgi processing was similar to the rapid Golgi procedure of Leeper (1978). Lizards were decapitated and the eyes enucleated. Eyecups were fixed in 2.5% glutaraldehyde overnight at 4°C, postfixed in 1% OsO_4 for 1 h at 4°C, then immersed in 0.3 M $K_2Cr_2O_7$ at room temperature for 2 weeks and gently agitated once a day. Eyecups were then transferred to fresh 1% $AgNO_3$ at room temperature for two days in darkness. The Golgi-stained eyecups were embedded in LX112-araldite resin (Ladd Inc., Burlington, Vermont). Golgi staining of flat-mounted retinas was not done because the retinal pigmented epithelium adheres very tightly to the cones in *Anolis* and removal caused excessive damage to the retina.

Resin embedded eyecups were sectioned radially on a sliding microtome at a thickness of 100–200 μm after warming the blockface with a tacking iron at 60–70°C (West 1972). The sections were remounted in fresh LX112-araldite resin between two sheets of clear plastic and polymerized.

(*c*) *Amacrine cell classification*

The functional organization of amacrine cells is highly correlated with dendritic organization in the

IPL, including arbor stratification pattern, depth and width (cf. Famiglietti *et al.* 1977; Teranishi *et al.* 1987; Ammermüller & Weiler 1989). Therefore, these dendritic characteristics, along with prominent somatic features, were used to classify cell types. Golgi-stained cells from four retinas were examined.

Cell classifications and morphometric measurements were made from camera lucida drawings of cells in thick sections. Each cell's cross-sectional somatic area, and major and minor soma axes were measured from digitized camera lucida drawings using NIH Image 1.40 software (National Institutes of Health, Bethesda, Maryland). Camera lucida drawings were digitized using a Hewlett-Packard ScanJet IIc flat bed scanner and Deskscan II software for the Apple MacIntosh personal computer. Morphometric measurements (table 2) were not corrected for tissue shrinkage. The actual amount of shrinkage in our Golgi-stained retinas is not known, but estimates of retinal shrinkage typically range from about 10–30% (Marc & Sperling 1976; Steinberg *et al.* 1973; Stone 1965). Easily identified *Anolis* amacrine cell types, such as interstitial amacrine cells and large ASP-IR amacrine cells, are of similar size in Golgi-stained and conventionally processed retinas used for immunocytochemistry (Sherry & Ulshafer 1992*a*,*b*; figure 6*h* and table 2 of this paper), indicating similar amounts of tissue shrinkage with both protocols.

Amacrine cell dendritic arbors were characterized according to dendritic stratification pattern, ramification depth in the IPL, amount of space occupied in the vertical dimension of the IPL ('extent'), density of arborization, dendritic morphology and field diameter.

Cells were first classified as stratified or non-stratified according to dendritic arborization pattern. Stratified cells were defined as having dendritic arbors with regions of increased bouton or process density at specific depths within the IPL. Stratified cells were further classified as mono-, bi- or tristratified according to the number of dendritic strata. The dendritic strata of multistratified amacrine cell types were numbered consecutively (D1,D2, etc.) beginning with the most distal stratum.

The midpoint depth of the dendritic ramification in the IPL (midpoint between the distal and proximal edges of a dendritic stratum) was determined for each dendritic stratum of all stratified cells and expressed as a percentage of IPL depth (distal and proximal IPL borders defined as 0% and 100%, respectively). The arbor depth of non-stratified cells was characterized as being confined to sublamina *a*, sublamina *b*, or spanning both sublaminae *a* and *b* of the IPL. Extent (the difference between the distal and proximal edges of a dendritic stratum) also was determined for each dendritic stratum of a cell and expressed as a percentage of total IPL width. Arborization density was characterized as dense or sparse according to the number of secondary dendrites and the presence or absence of boutons was noted.

The dendritic fields of Golgi-stained cells were categorized according to the scheme used to classify turtle amacrine cells (Kolb 1982), with the addition of a very narrow field category as follows: very narrow field (< 30 μm diameter); narrow field (30–150 μm diameter); small field (150–300 μm diameter); medium field (300–500 μm diameter); wide field (> 500 μm diameter). As Golgi-stained amacrine cells were studied in radial sections 100–200 μm thick, the dendritic arbors of many cells, particularly those with large fields, were truncated by sectioning and definitive measurement of dendritic field diameter was impossible in many cases. Cases where the dendritic arbors were truncated are noted in the text, and dendritic field diameter values presented for such cell types should be regarded as estimates of the minimum field width.

Somatic features examined included soma morphology (pyriform versus multipolar), location and size. Cells with somas in the ganglion cell layer (GCL) and no axon were classified as displaced amacrine cells.

Nomenclature was adopted as follows. Cells were designated as amacrine cells by the prefix 'A' (Kolb 1982), followed by a stratification designation: N, non-stratified; M, monostratified; B, bistratified; or T, tristratified. A numeral was assigned to designate each cell type within a stratification class. Cells with similar somatic and dendritic features but differing in IPL ramification depth were grouped together as subtypes of a single type, a strategy used by Ramon y Cajal (1933) and more recently by Wagner & Wagner (1988) in fish retina. Such stratification subtypes were designated by a number following a decimal point and were numbered from distal to proximal. For example, a cell designated as AM3.1 would be a type 3 monostratified amacrine cell of the most distal subtype.

(*d*) *Neurotransmitter identification*

GABA, GLY and ASP content in Golgi-stained amacrine cells was demonstrated immunocytochemically using a Golgi–postembedding immunofluorescence procedure (Sherry & Yazulla 1993*b*). All neurotransmitter identification experiments were done on Golgi-stained cells that had been classified according to morphology prior to immunocytochemistry (ICC). The reader is referred to Sherry & Yazulla (1993*b*) for the technical and specificity details of the Golgi–ICC technique used here. Briefly, Golgi-stained cells of interest were cut from thick resin sections and remounted on plastic stubs for semithin sectioning. Serial semithin sections (1 μm thick) were mounted on gelatin coated glass slides for immunocytochemistry. Sections containing the nucleus of the Golgi-stained cell were tested for GABA-immunoreactivity (IR). Serial sections of many cells were also tested for GLY-IR and ASP-IR. Immunoreacted semithin sections were photographed using combined ultraviolet and bright field illumination to show immunofluorescence in the nucleus and Golgi deposits in the cytoplasm simultaneously.

Rabbit polyclonal antisera directed against glutaraldehyde conjugates of GABA, GLY and ASP were the gift of Robert Wenthold (anti-GABA and anti-GLY) or purchased from Chemicon International (Lomita, California; anti-GABA and anti-ASP). All

antisera were highly specific for the conjugate they were raised against as reported previously (Wenthold *et al.* 1986, 1987; Sherry & Ulshafer 1992*a*,*b*), and we use the terms GABA-, GLY- and ASP-IR, rather than GABA-, GLY- or ASP-like immunoreactivity. Secondary antiserum was goat anti-rabbit conjugated to fluorescein isothiocyanate (GAR-FITC, Boeringer-Mannheim, Indianapolis, Indiana). Antisera were used at the following dilutions: anti-GABA, 1:1500; anti-GLY, 1:100; anti-ASP, 1:1000; and GAR-FITC, 1:30. All sera were diluted in 2% normal goat serum in phosphate buffered saline (PBS, pH 7.4). Substitution of normal rabbit serum for the primary antiserum eliminated all specific immunolabelling.

The intensity of GLY-IR, which in reptilian retinas is high in peripheral retina but considerably lower in central retina (Eldred & Cheung 1989; Sherry *et al.* 1993), made detection of GLY-IR containing amacrine cells difficult in central retina. Many of the Golgi-stained amacrine cells with the morphological features of GLY-containing cells were located in central retina, and required improved GLY-IR visualization. Visualization of GLY-IR was improved in several experiments by replacing PBS with a high salt tris buffer (0.05 M Tris plus 1.5% NaCl and 0.02% Tween 20; pH 7.6 at 24°C) for all rinses and high salt tris buffer plus 4% NGS and 4% dry milk for the initial blocking step and primary antiserum dilution. The procedure and antiserum used to visualize GLY-IR were identical to those above.

Several cells showed nuclear IR intensity levels that were difficult to characterize. In these cases, micrographs of the cells were digitized as described above and the intensity of IR in the Golgi-stained cell was compared to the background IR intensity of the same section using the thresholding function of the NIH Image 1.40 program. Because *Anolis* bipolar and Müller cells do not contain specific GABA-IR or GLY-IR (Sherry & Ulshafer 1992*a*; Sherry *et al.* 1993), IR levels over these cells was defined as background. If thresholding revealed that the nuclear IR intensity was greater than background IR intensity, the cell was scored as positive.

(*e*) *Neurotransmitter-related enzyme localization*

In conjunction with Golgi–ICC experiments, localization of glutamic acid decarboxylase (GAD, the synthetic enzyme for GABA) and colocalization of GABA and tyrosine hydroxylase (TOH, the synthetic enzyme for catecholamines), were examined immunocytochemically in conventionally processed, resin embedded retinas. Tissue used for these experiments was fixed overnight in 2.0% paraformaldehyde plus 0.5% glutaraldehyde and embedded in LX112-araldite resin polymerized at 40°C. Immunoreactivity was visualized using postembedding immunofluorescence (Sherry & Ulshafer 1992*a*,*b*). Demonstration of GAD-IR required the background reduction steps used for GLY-IR. Colocalization of TOH-IR and GABA-IR was determined by examining TOH-IR containing cells on serial 1 μm semithin sections reacted for GABA-IR. The rabbit polyclonal serum raised against bovine TOH was a gift from T. Joh (Joh *et al.* 1973). Rabbit polyclonal antisera raised against catfish GAD were the gift of J.-Y. Wu (Su *et al.* 1979).

3. RESULTS

A total of 186 Golgi-stained amacrine cells from four retinas were characterized morphologically. Twenty three cell types were identified, including non-, mono-, bi- and tristratified types. Immunocytochemistry was performed on 65 Golgi-stained amacrine cells to determine GABA, GLY and ASP content. Immunocytochemical experiments were structured so that examples of all 23 morphological cell types were tested, and all cells tested for GLY-IR were also tested for GABA-IR to allow assessment of GABA–GLY colocalization (table 1). The morphological character-

Table 1. *Numbers of Golgi-stained* Anolis *amacrine cells and cell types tested for GABA-IR, GLY-IR and ASP-IR*

(*a*) Data by numbers of cells

	no. cells tested for:			no. cells (+) for:		
	GABA-IR	GLY-IR	ASP-IR	GABA-IR	GLY-IR	ASP-IR
monostrat.	43	35	18	38	7	0
bistrat.	10	8	0	8	0[a]	0
tristrat.	8	8	0	1	7	0
non-strat.	4	3	0	3	1	0
total no. tested or (+)	65	54	18	50	15[a]	0

(*b*) Data by cell type

	no. cell types tested for:			no. cell types (+) for:		
	GABA-IR	GLY-IR	ASP-IR	GABA-IR	GLY-IR	ASP-IR
monostrat.	13	13	3	11	1	0
bistrat.	5	5	0	3	0[a]	0
tristrat.	2	2	0	1	1	0
non-strat.	3	3	0	2	1	0
total no. tested or (+)	23	23	3	17	3[a]	0
percentage of all types	100	100	13.0	73.9	13.0	0

[a] GLY-IR content uncertain for some types; see text.

Table 2. *Morphological data for* Anolis *amacrine cell types*
(All values = mean ± standard deviation.)

	AM1	AM2	AM3.1	AM3.2	AM4	AM5
sample size (*n*)	6	3	2	12	1	1
soma morphology	pyriform	pyriform	pyriform	pyriform	pyriform	pyriform
soma location[a]	proximal	proximal	proximal	proximal	distal	distal
soma area/μm²	62.0 ± 19.3	86.9 ± 12.8	117.4	54.3 ± 14.6	60.2	70.6
soma major axis/μm	10.6 ± 3.4	12.5 ± 1.9	13.9	9.4 ± 1.6	9.4	10.0
soma minor axis/μm	7.6 ± 0.9	8.9 ± 0.6	10.7	7.3 ± 0.9	8.2	9.0
no. primary dendrites	1	1	1	1	1	1
primary dendrite diam.	slender	medium	medium	medium	medium	medium
dendritic plexus	dense	dense	very sparse	very sparse	dense	sparse
boutons	yes	yes	no	no	yes	no
stratification midpoint (% IPL depth)						
D1	14.3 ± 2.8	44.6 ± 2.7	0	84.1 ± 8.7	11.1	14.5
D2	—	—	—	—	—	—
D3	—	—	—	—	—	—
stratum extent (% IPL depth spanned)						
D1	15.0 ± 3.3	22.9 ± 3.4	0	12.3 ± 3.5	9.5	13.2
D2	—	—	—	—	—	—
D3	—	—	—	—	—	—
dendritic field class	very narrow	small	med-wide	wide	small	small
maximum field diam./μm						
D1	33.3	256.0	194.6[b]	791.0 radius	197.1	207.4
D2	—	—	—	—	—	—
D3	—	—	—	—	—	—

	AM6	AM7.1	AM7.2	AM7.3	AM8	AM9.1
sample size (*n*)	2	6	3	5	3	1
soma morphology	pyriform	pyriform	pyriform	pyriform	pyriform	pyriform
soma location	distal	proximal	proximal	proximal	proximal	distal
soma area/μm²	77.1	76.4 ± 21.0	119.6 ± 8.8	85.3 ± 22.6	113.9 ± 23.1	78.0
soma major axis/μm	13.8	11.8 ± 1.3	15.1 ± 2.0	11.5 ± 1.3	16.2 ± 1.6	14.2
soma minor axis/μm	7.1	8.4 ± 1.2	10.2 ± 1.7	9.3 ± 1.4	9.2 ± 1.2	7.2
no. primary dendrites	1	1	1	1	1	1
primary dendrite diam.	medium	medium	medium	medium	large	large
dendritic plexus	dense	sparse	sparse	sparse	sparse	dense
boutons	yes	yes	yes	yes	no	yes
stratification midpoint (% IPL depth)						
D1	12.7	43.6 ± 5.6	64.3 ± 4.8	87.2 ± 4.1	87.4 ± 1.9	15.8 ± 1.1
D2	—	—	—	—	—	—
D3	—	—	—	—	—	—
stratum extent (% IPL depth spanned)						
D1	10.0	10.4 ± 3.9	9.5 ± 2.2	17.3 ± 5.7	10.9 ± 5.2	9.6 + 0.9
D2	—	—	—	—	—	—
D3	—	—	—	—	—	—
dendritic field class	?	med-wide	wide	?	?	?
maximum field diam./μm						
D1	64.0[b]	358.4	524.8	163.8[b]	195.8[b]	[b]
D2	—	—	—	—	—	—
D3	—	—	—	—	—	—

Table 2. *Continued*

	AM9.2	AM9.3	AM9.4	AM10.1	AM10.2	AM11
sample size (*n*)	1	4	2	44	30	7
soma morphology	pyriform	pyriform	pyriform	pyriform	pyriform	columnar
soma location	distal	distal	distal	variable	variable	proximal
soma area/μm^2	103.6	96.9 ± 30.9	104.0	117.8 ± 22.7	121.3 ± 16.5	121.9 ± 16.6
soma major axis/μm	14.5	15.1 ± 3.2	16.6	14.0 ± 1.5	14.5 ± 1.2	15.3 ± 1.8
soma minor axis/μm	9.1	8.1 ± 1.2	7.9	10.7 ± 1.3	10.7 ± 1.2	10.2 ± 1.4
no. primary dendrites	1	1	1	1	1	1
primary dendrite diam.	large	large	large	large	large	very large
dendritic plexus	dense	dense	dense	dense	dense	sparse
boutons	yes	yes	yes	yes	yes	no
stratification midpoint (% IPL depth)						
D1	31.2	61.0 ± 2.1	81.1	18.0 ± 4.8	66.8 ± 4.7	37.7 ± 4.6
D2	—	—	—	—	—	—
D3	—	—	—	—	—	—
stratum extent (% IPL depth spanned)						
D1	15.1	10.4 ± 1.8	14.9	14.6 ± 4.7	14.8 ± 3.9	12.4 ± 3.5
D2	—	—	—	—	—	—
D3	—	—	—	—	—	—
dendritic field class	?	?	med-wide	wide	wide	med-wide
maximum field diam./μm						
D1	[b]	[b]	297.0[b]	847.4	727.0	366.1[b]
D2	—	—	—	—	—	—
D3	—	—	—	—	—	—

	AM12	AM13	AB1	AB2	AB3	AB4.1
sample size (*n*)	6	6	1	5	6	4
soma morphology	interstitial	multipolar	pyriform	pyriform	multipolar	multipolar
soma location	mid IPL	proximal	distal	proximal	proximal	proximal
soma area/μm^2	153.8 ± 28.6	91.4 ± 29.8	25.4	58.7 ± 4.7	114.4 ± 29.1	93.8 ± 28.0
soma major axis/μm	16.0 ± 1.3	12.0 ± 1.8	8.4	10.2 ± 1.4	14.0 ± 1.7	12.0 ± 1.8
soma minor axis/μm	12.2 ± 1.9	9.5 ± 1.8	5.2	7.4 ± 0.4	10.4 ± 1.6	9.8 ± 1.3
no. primary dendrites	2–4	2–4	1	1	2–4	2–4
primary dendrite diam.	very large	medium	slender	medium	medium	medium
dendritic plexus	sparse	sparse	dense	sparse	sparse	sparse
boutons	no	no	yes	no	no	no
stratification midpoint (% IPL depth)						
D1	41.8 ± 4.4	14.0 ± 4.0	—	25.2 ± 6.2	15.8 ± 3.8	9.4 ± 3.7
D2	—	—	—	82.0 ± 4.5	43.8 ± 2.2	84.1 ± 1.1
D3	—	—	—	—	—	—
stratum extent (% IPL depth spanned)						
D1	20.3 ± 2.0	13.5 ± 3.2	—	21.1 ± 10.5	11.1 ± 3.3	10.5 ± 2.6
D2	—	—	—	23.4 ± 8.8	15.4 ± 2.8	21.1 ± 3.9
D3	—	—	—	—	—	—
dendritic field class	wide	wide	very narrow	narrow	med-wide	med-wide
maximum field diam./μm						
D1	458.2[b]	455.7[b]	11.3	66.6	410.0	273.9
D2	—	—	8.8	76.8	312.3	317.4
D3	—	—	—	—	—	—

Table 2. *Continued*

	AB4.2	AB5	AT1	AT2	AN1	AN2	AN3
sample size (*n*)	3	1	11	1	4	2	3
soma morphology	pyriform	pyriform	pyriform	multipolar	pyriform	pyriform	pyriform
soma location	proximal	displaced	distal	proximal	distal	distal	proximal
soma area/μm^2	89.9 ± 8.0	26.1	25.2 ± 4.8	96.6	32.2 ± 10.1	34.9	79.2 ± 26.7
soma major axis/μm	12.3 ± 1.2	7.6	7.9 ± 1.0	11.3	8.2 ± 2.0	8.5	11.5 ± 1.3
soma minor axis/μm	9.4 ± 1.0	4.4	5.2 ± 0.7	10.9	6.0 ± 0.9	7.5	8.6 ± 2.1
no. primary dendrites	1	1	1	3	1	1	1
primary dendrite diam.	medium	slender	slender	medium	slender	slender	medium
dendritic plexus	sparse	dense	dense	sparse	sparse	sparse	very sparse
boutons	no	yes	yes	no	yes	yes	yes
stratification midpoint (% IPL depth)							
D1	5.6 ± 1.8	46.6	16.5 ± 1.7	15.2	sub *a*	sub *a*/*b*	sub *a*
D2	87.9 ± 1.8	61.4	42.7 ± 1.6	57.6	—	—	—
D3	—	—	61.8 ± 2.3	87.0	—	—	—
stratum extent (% IPL depth spanned)							
D1	7.7 ± 2.3	11.4	8.1 ± 1.1	13.0	52.6 ± 5.8	87.9	49.1 ± 5.9
D2	18.8 ± 2.4	4.5	10.5 ± 1.4	10.9	—	—	—
D3	—	—	7.4 ± 1.3	17.4	—	—	—
dendritic field class	?	narrow	very narrow	med-large	very narrow	very narrow	narrow
maximum field diam./μm							
D1	51.2[b]	62.7	25.0	209.2	25.0	28.8	107.5
D2	113.9[b]	35.8	32.5	172.8	—	—	—
D3	—	—	20.0	247.0	—	—	—

[a] Soma location within amacrine cell layer of INL.
[b] Indicates highly truncated dendritic field.

istics of all 23 amacrine cell types are summarized in table 2.

The distribution of GABA-IR, GLY-IR and ASP-IR in Golgi-stained *Anolis* retina was similar to that seen in conventionally processed *Anolis* retina (Sherry & Ulshafer 1992*a*,*b*; Sherry *et al.* 1993), including IPL stratification. The GABA-IR and GLY-IR stratification patterns in the IPL were often difficult to resolve in micrographs using combined fluorescence and brightfield illumination. However, in many micrographs four GABA-IR laminae are visible in the IPL (for example, figure 4*a*) similar to conventionally processed *Anolis* retina (Sherry *et al.* 1993). The stratification pattern of GLY-IR in the IPL of Golgi-stained retinas is more difficult to discern due to the lower overall intensity of GLY-IR, but weak GLY-IR stratification is visible in some cases (for example, figure 6*g*).

(*a*) *Monostratified cell types*

Monostratified cells comprised 13 types and represented the majority of cells ($n = 145$). Monostratified cells showed great heterogeneity in somatic and dendritic characteristics, and included pyriform and multipolar types and field diameters ranging from very narrow to wide. Several monostratified cell types had similar somatic features but could be distinguished on the basis of dendritic characteristics.

(i) *Type AM1*

This cell type ($n = 6$) was easily identified by its dendrites, which formed a very narrow, dense cloud of boutons centred at about 15% IPL depth (figures 1*a* and 2). Average dendritic field diameter for this cell type was 26.1 ± 4.6 μm. Processes from other Golgi-stained stratified amacrine cell types passed through the boutons of AM1 cells (figure 1*a*) which had round pyriform somas located in the most proximal INL. Both AM1 cells tested contained GABA-IR (figure 4*a*), but not GLY-IR.

(ii) *Type AM2*

Cells of the AM2 cell type ($n = 3$; figures 1*b* and 2) had relatively large, pyriform somas in the proximal INL. The dendrites of AM2 cells had numerous boutons and a relatively broad extent in the mid IPL. The field diameter of AM2 cells was in the small category. The one AM2 cell tested contained GABA-IR (figure 4*b*), but not GLY-IR.

(iii) *Type AM3*

Cells of the AM3 type ($n = 14$; figure 1*c* and 2) comprised two subtypes; one ramified at the INL–IPL border (AM3.1) and one ramified deep in the proximal IPL (AM3.2). The pyriform somas of AM3 cells were located in the proximal INL and gave rise to a single descending process. The dendritic field of AM3 cells was characterized by its linear organization. The

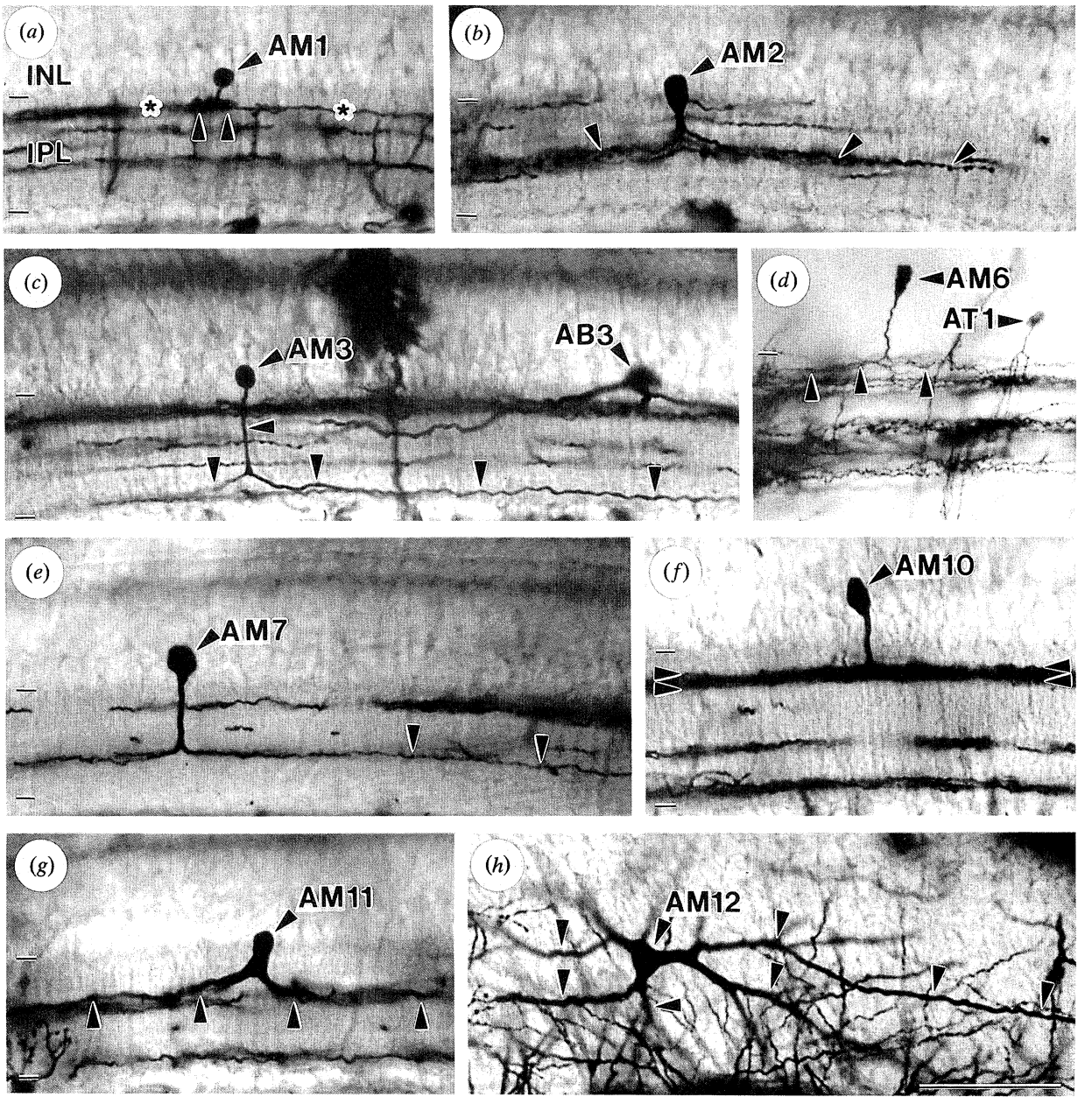

Figure 1. Golgi impregnated monostratified amacrine cells. Tick marks show the borders of the IPL. (*a*) AM1 cell with its characteristic cloud of boutons (arrowheads). Golgi-stained processes from other cells (asterisks) pass through the boutons. (*b*) AM2 cell with its bouton-bearing dendrites ramifying in the mid IPL (arrowheads). (*c*) AM3 cell of the AM3.2 subtype with a relatively thick primary dendrite and secondary dendrites coursing in opposite directions deep within the IPL (arrowheads). A bistratified AB3 cell is also present. (*d*) AM6 cell with its distally placed, rhomboidal soma. This cell gives rise to several fine dendrites in the distal IPL (arrowheads). A Golgi-stained AT1 cell also is present. (*e*) AM7 cell of the AM7.2 subtype. These cells are characterized by a pyriform soma, a relatively thick descending dendrite and few secondary dendrites with boutons (arrowheads). (*f*) AM10 cell of the AM10.1 subtype, with a distally placed soma, thick descending dendrite and dense plexus of secondary dendrites in the distal IPL (arrowheads). (*g*) AM11 cell with the characteristic cylindrical soma and stout, sparsely branched dendrites (arrowheads). (*h*) AM12 interstitial amacrine cell seen in tangential section. The soma is contained within the depth of the IPL and gives rise to several stout, sparsely branched dendrites (arrowheads). Calibration bar = 50 μm for all micrographs.

descending dendrite bifurcated into two secondary dendrites coursing at 180° to one another with little or no branching. The largest AM3.1 dendritic field was measured at about 200 μm in diameter, but was truncated. The fields of several AM3.2 cells were less severely truncated, with the maximal diameter measured at about 450 μm. However, one secondary dendrite of an AM3.2 cell was traced over 790 μm, indicating these are wide field cells. Both AM3.1 cells and four AM3.2 cells were tested for GABA and GLY content and showed only GABA-IR (figure 4*c*). Both AM3.1 cells were also negative for ASP-IR.

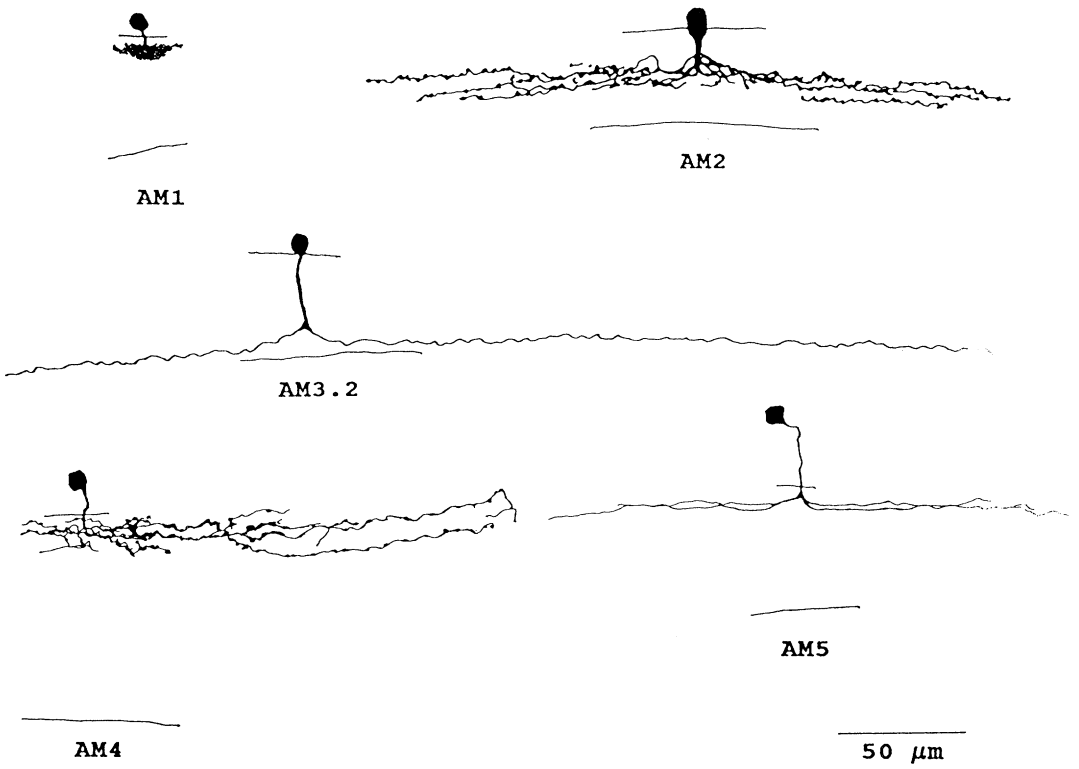

Figure 2. Camera lucida drawings of AM1, AM2, AM3.2, AM4 and AM5 amacrine cells. All drawings to same scale.

(iv) *Type AM4*

The AM4 cell type was composed of a single cell located in the parafoveal region (figure 2). The small pyriform soma of this cell was located distal to the INL–IPL border. The dendrites of this cell were fine and the numerous secondary dendrites ramified in the distal IPL and had many boutons. The field of this cell may have been slightly truncated, but appeared to be in the small category. The cell did not show GABA-IR or GLY-IR.

(v) *Type AM5*

The AM5 cell type also was composed of a single small pyriform cell from the parafoveal region (figure 2). The AM5 cell was distinguished from the AM4 cell by having only four secondary dendrites which did not have boutons. The field of the AM5 cell also fell into the small category and probably was truncated slightly by sectioning. The cell did not show GABA-IR or GLY-IR.

(vi) *Type AM6*

The AM6 cell type ($n=2$; figures 1*d* and 3) was characterized by its distally placed, somewhat rhomboidal pyriform soma. The soma and primary dendrite of AM6 cells were of medium size. The primary dendrite gave rise to a number of secondary dendrites ramifying in the distal IPL. Both AM6 cells ramified in a region of the IPL that contained numerous other Golgi-stained processes making it impossible to determine the diameter of the dendritic field. The AM6 cell tested showed GABA-IR (figure 4*d*) but not GLY-IR.

(vii) *Type AM7*

The AM7 cells ($n=14$; figures 1*e* and 3) comprised three stratification subtypes; AM7.1 ramified at about 45% IPL depth, AM7.2 ramified at about 65% IPL depth and AM7.3 ramified at about 85% IPL depth. These cells possessed a medium to large pyriform soma in the proximal INL. The primary dendrite was of medium diameter and gave rise to a sparse ramification of secondary dendrites. Boutons were present on the distal portion of the secondary dendrites. The fields of these cells were relatively large, and as a result the fields were somewhat truncated. However, several fields exceeding 300 μm were measured and one field exceeded 500 μm, indicating that AM7 cells are probably wide field cells. All five AM7 cells tested showed GABA-IR (figure 4*e*) and included all three subtypes. Two cells were tested for GLY-IR, but neither cell showed GLY-IR. The AM7 cell type showed similarities to one ASP-IR *Anolis* amacrine cell type (Sherry & Ulshafer 1992*b*), but no Golgi-stained AM7 cells showed ASP-IR.

(viii) *Type AM8*

The AM8 cell type ($n=3$; figure 3) was identified by its large, pyriform soma which protruded into the IPL and the large primary dendrite which descended deep into the IPL before giving rise to a sparse ramification of large secondary dendrites. No boutons were seen on the secondary dendrites. The field size of this cell type is uncertain because all fields measured were highly truncated, but certainly exceeds the 195 μm diameter measured for the largest field. The AM8 cell tested showed GABA-IR but not GLY-IR.

(ix) *Type AM9*

The AM9 cell type comprised four stratification subtypes (AM9.1–9.4; total $n=8$) and was character-

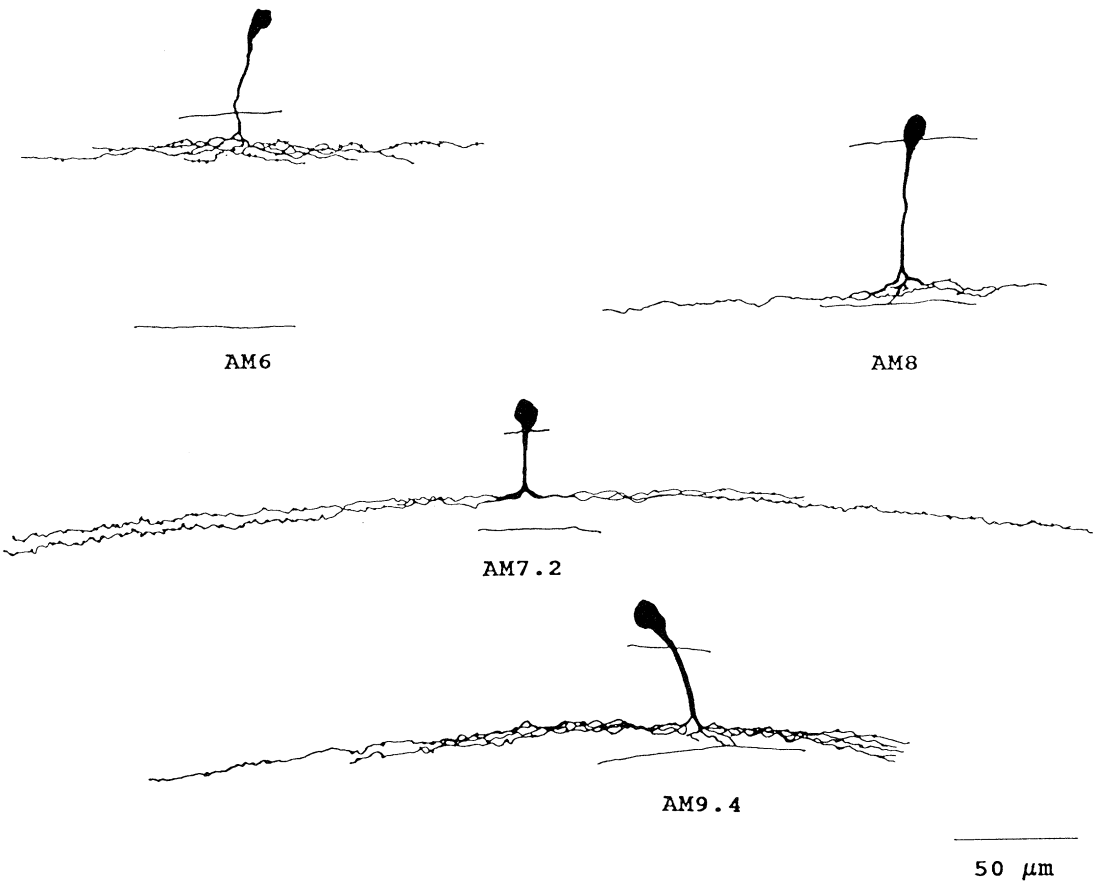

Figure 3. Camera lucida drawings of AM6, AM7.2, AM8 and AM9.4 cells. All drawings to same scale.

ized by a relatively large, distally placed pyriform soma that often had an irregular outline (figure 3). The large primary dendrite descended to the level of ramification and gave rise to a dense plexus of secondary dendrites, which often had boutons. Cells with striking morphological similarities to Golgi-stained AM9 cells show GABA-IR in conventionally processed *Anolis* retina (Sherry & Ulshafer 1992*a*). Six AM9 cells, including cells of all four subtypes, were tested for both GABA-IR and GLY-IR. The intensity of nuclear GABA-IR in AM9 cells was characteristically quite low, but computer-assisted intensity thresholding confirmed that the GABA-IR intensity in five of the six AM9 cells was slightly above background intensity (figure 4*f*). Non-impregnated amacrine cells similar to AM9 cells in size, location and appearance, often showed intense cytoplasmic GABA-IR and low nuclear GABA-IR (figure 4*f*). We concluded from these results that AM9 cells were a GABA-IR type, but the nuclear pool of GABA in AM9 cells may be particularly sensitive to steps in the Golgi impregnation, embedding or immunocytochemical procedures. No AM9 cells showed GLY-IR.

(x) *Type AM10*

Type AM10 cells were the most frequently encountered cells ($n = 74$; figures 1*f* and 5) and comprised two subtypes; one ramified at about 20% IPL depth and one ramified at about 70% IPL depth. Both subtypes had large pyriform somas with proximal to distal placement in the INL. The descending process was large and gave rise to a dense ramification of secondary dendrites, which often had boutons. These cells were often encountered together and the dendritic fields of neighboring cells showed considerable overlap, making tracing the dendrites very difficult. Dendritic field size for AM10 cells was in the wide category, as fields measured for both subtypes exceeded 500 μm.

The GABA-IR and GLY-IR labelling patterns in this cell type were complex suggestive of neurochemical heterogeneity within this morphological type (table 3 and figure 6). Fourteen cells, seven of each subtype, were tested for both GABA-IR and GLY-IR. Three neurochemical classes of AM10 cell were identified on the basis of GABA-IR and GLY-IR content: cells containing GABA-IR only; cells containing GABA-IR and GLY-IR; and cells that contained neither GABA-IR nor GLY-IR. Cells showing neither GABA-IR nor GLY-IR were found only within the AM10.1 subtype, but GABA-IR only and GABA-IR–GLY-IR cells of both subtypes were seen. No AM10 cells showed only GLY-IR. *Anolis* AM10 cells represent a portion of the *Anolis* $A1_2$ cell population, which includes GABA-IR only and GABA-IR–GLY-IR cells in conventionally processed retina (Sherry & Ulshafer 1992*a*; Sherry *et al.* 1993), consistent with the results obtained in Golgi-stained AM10 cells.

The AM10 cells showed morphological similarities to some ASP-IR *Anolis* amacrine cells (Sherry & Ulshafer 1992*b*) and all 14 AM10 cells were also tested for ASP-IR. No AM10 cells showed ASP-IR, indicat-

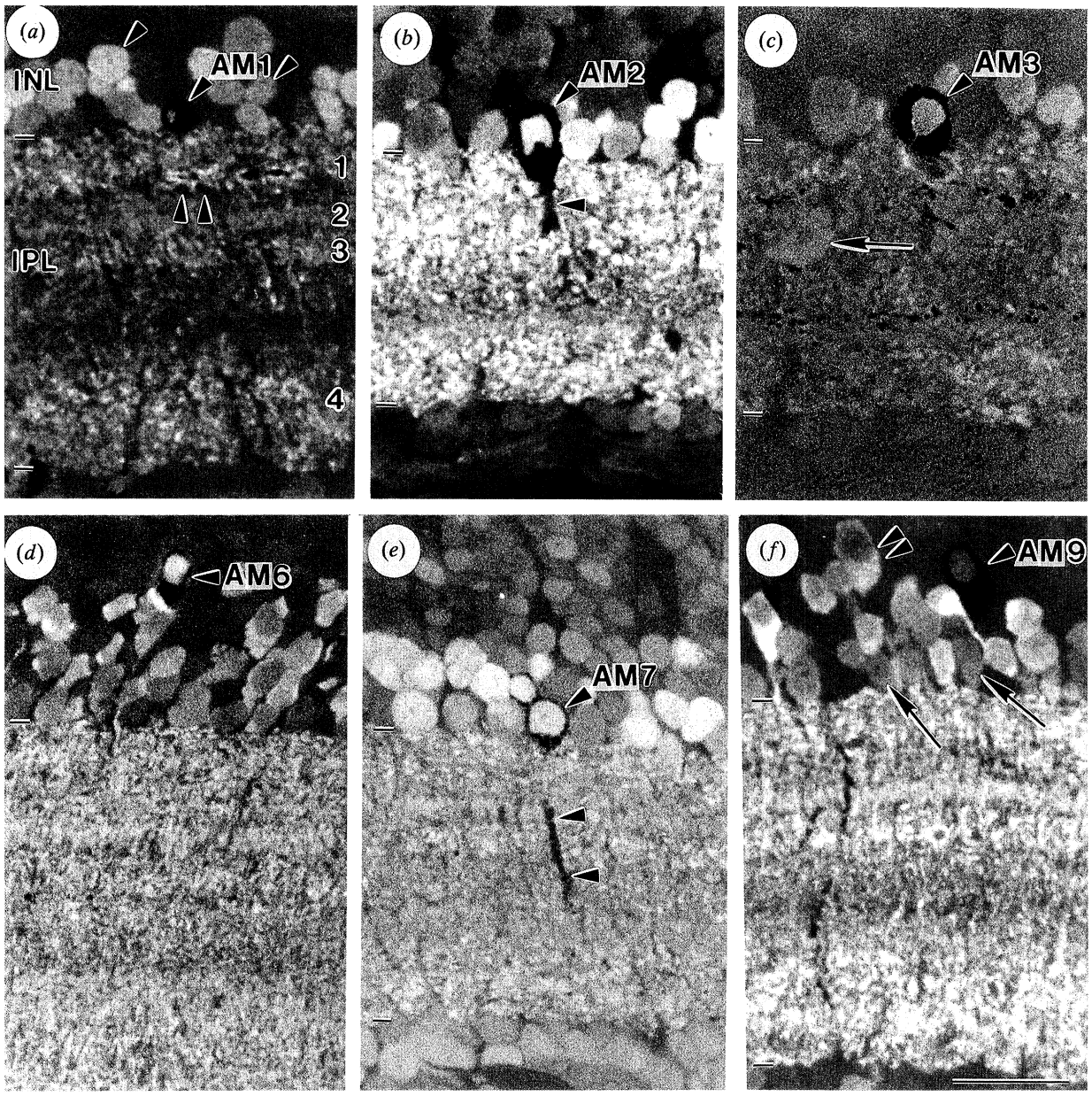

Figure 4. Combined bright field-fluorescence micrographs of several GABA-IR monostratified amacrine cell types. (*a*) GABA-IR in the nucleus of a Golgi impregnated AM1 cell. Single arrowheads show other non-impregnated GABA-IR amacrine cells. Double arrowheads in the IPL show some boutons from the AM1 cell's dendrites. GABA-IR in the IPL shows the typical four layered pattern (1–4). (*b*) Intense GABA-IR in an AM2 cell. The descending dendrite of the cell is also visible (arrowhead). (*c*) Double-labelled AM3 cell of the AM3.1 cell type. A non-impregnated GABA-IR interstitial cell is visible in the IPL (arrow). Note, the Golgi deposits in the distal IPL are not from the AM3.1 cell shown. (*d*) A double-labelled AM6 cell. Note the distal placement of the soma. (*e*) An example of a GABA-IR AM7.3 cell. Part of the cell's descending process is visible in the IPL (arrowheads). (*f*) GABA-IR in the nuclei of AM9 cells is typically weak, but computer-assisted thresholding shows these GABA-IR levels to be above background and similar in intensity to other weakly GABA-IR cells (arrows). A non-impregnated cell similar in appearance to the AM9 cell that shows strong somatic GABA-IR and weak nuclear GABA-IR is also visible (double arrowheads). Calibration bar = 20 μm.

ing that the ASP-IR *Anolis* amacrine cells and AM10 cells are separate populations (figure 6*e*,*h*).

(xi) *Type AM11*

This cell type ($n = 7$; figures 1*g* and 7) was very distinctive in its appearance and ramified at about 40% IPL depth. The cylindrical somas of AM11 cells were located at the INL–IPL border. The descending process showed little narrowing as it descended into the IPL where it gave rise to a sparse ramification of very thick secondary dendrites that showed little branching and no boutons. The largest field measured for an AM11 cell was a little over 350 μm but was truncated, and these cells probably possess wide dendritic fields. Both AM11 cells tested showed GABA-IR (figure 8*a*), but the cell tested for GLY-IR did not show labelling.

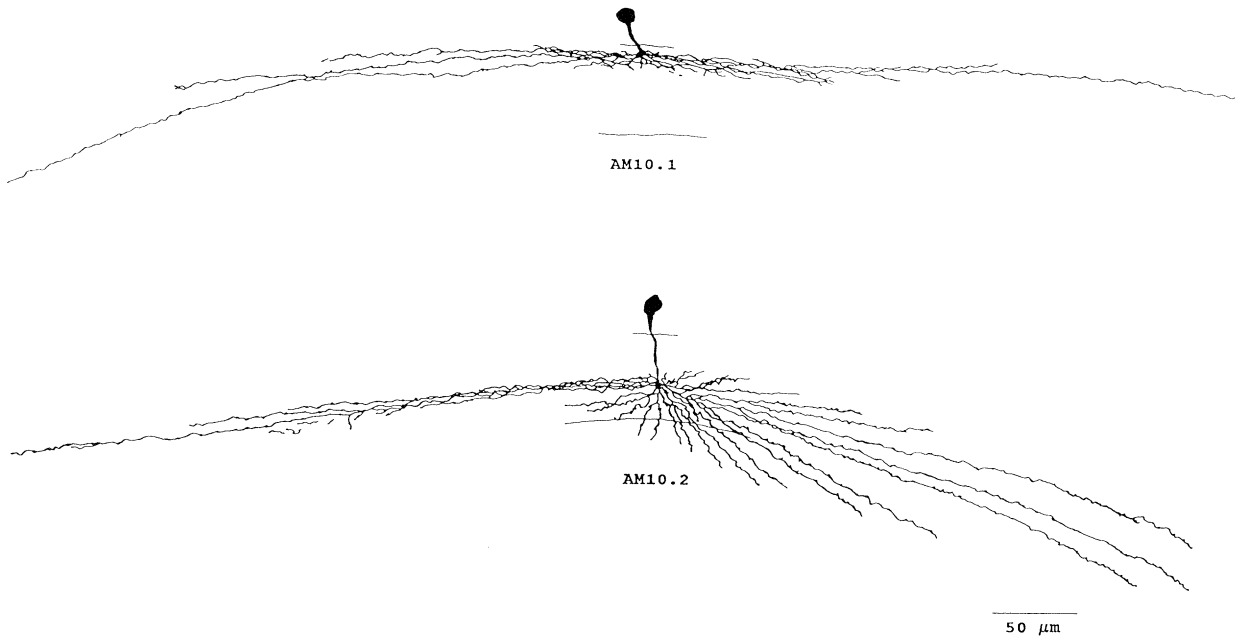

Figure 5. Camera lucida drawings of AM10.1 and AM10.2 cells. The dendrites of the AM10.2 cell become somewhat oblique to the right of the figure. Both cells are drawn to the same scale.

(xii) *Type AM12*

Type AM12 cells ($n=6$; figures 1*h* and 7) were the only type of interstitial cell observed. The rounded or pyramidal somas of AM12 cells were located in sublamina *a* of the IPL and gave rise to two to four stout dendrites from the proximal side. The dendrites showed little branching and no boutons. An interesting feature observed on this cell was that the thick primary dendrites suddenly narrowed and continued as a fine process. One tangentially oriented AM12 cell with a truncated dendritic field of over 450 μm was encountered, indicating that these cells are wide field cells. Both AM12 cells tested showed strong GABA-IR (figure 8*b*), but no GLY-IR was seen in the one cell tested.

(xiii) *Type AM13*

Type AM13 cells ($n=6$; figure 7) were characterized by a rounded or fusiform multipolar soma in the most proximal INL that gave rise to two to four primary dendrites of medium diameter. The dendrites showed relatively little branching and all AM13 cells ramified at about 15% IPL depth. One AM13 cell had a truncated dendritic field diameter of over 450 μm, and these cells are also probably a wide field type. The two AM13 cells tested both showed GABA-IR (figure 8*c*), but the cell tested for GLY-IR did not show labelling.

(*b*) *Bistratified amacrine cell types*

Bistratified amacrine cells ($n=20$) comprised five types and showed diverse dendritic and somatic characteristics.

(i) *Type AB1*

A single example of the AB1 cell was characterized by a very narrow dendritic field with two layers of very dense boutons (figure 10). The cell was oriented somewhat obliquely, but one stratum of boutons was clearly in sublamina *a* of the IPL and the second tier of boutons was in the mid IPL. The soma of this cell was small and pyriform in shape and was located well distal to the INL–IPL border. The cell did not show GABA-IR. Determination of GLY-IR content was hampered by the cell's central location and small soma. It is not clear if the AB1 cell is a GLY-IR containing type, but given the similarities between this cell type and GLY-IR amacrine cells seen in conventionally processed *Anolis* retina (Sherry *et al.* 1993) it is possible that the AB1 cell type contains GLY.

(ii) *Type AB2*

Cells of the AB2 type ($n=5$; figures 9*a* and 10) were characterized by medium sized pyriform somas located

Table 3. *Neurotransmitter heterogeniety of Golgi-stained* Anolis *AM10 amacrine cells*

	AM10.1		AM10.2	
	number	percent	number	percent
cells tested	7	100	7	100
GABA-IR(+)	5	71.4	7	100
GABA-IR(−)	2	28.6	0	0
GLY-IR(+)	3	42.9	4	57.1
GLY-IR(−)	4	57.1	3	42.9
ASP-IR(+)	0	0	0	0
ASP-IR(−)	0	0	0	0
GABA-IR(+) only	2	28.6	3	42.9
GLY-IR(+) only	0	0	0	0
GABA/GLY-IR(+)	3	42.9	4	57.1
GABA/GLY-IR(−)	2	28.6	0	0

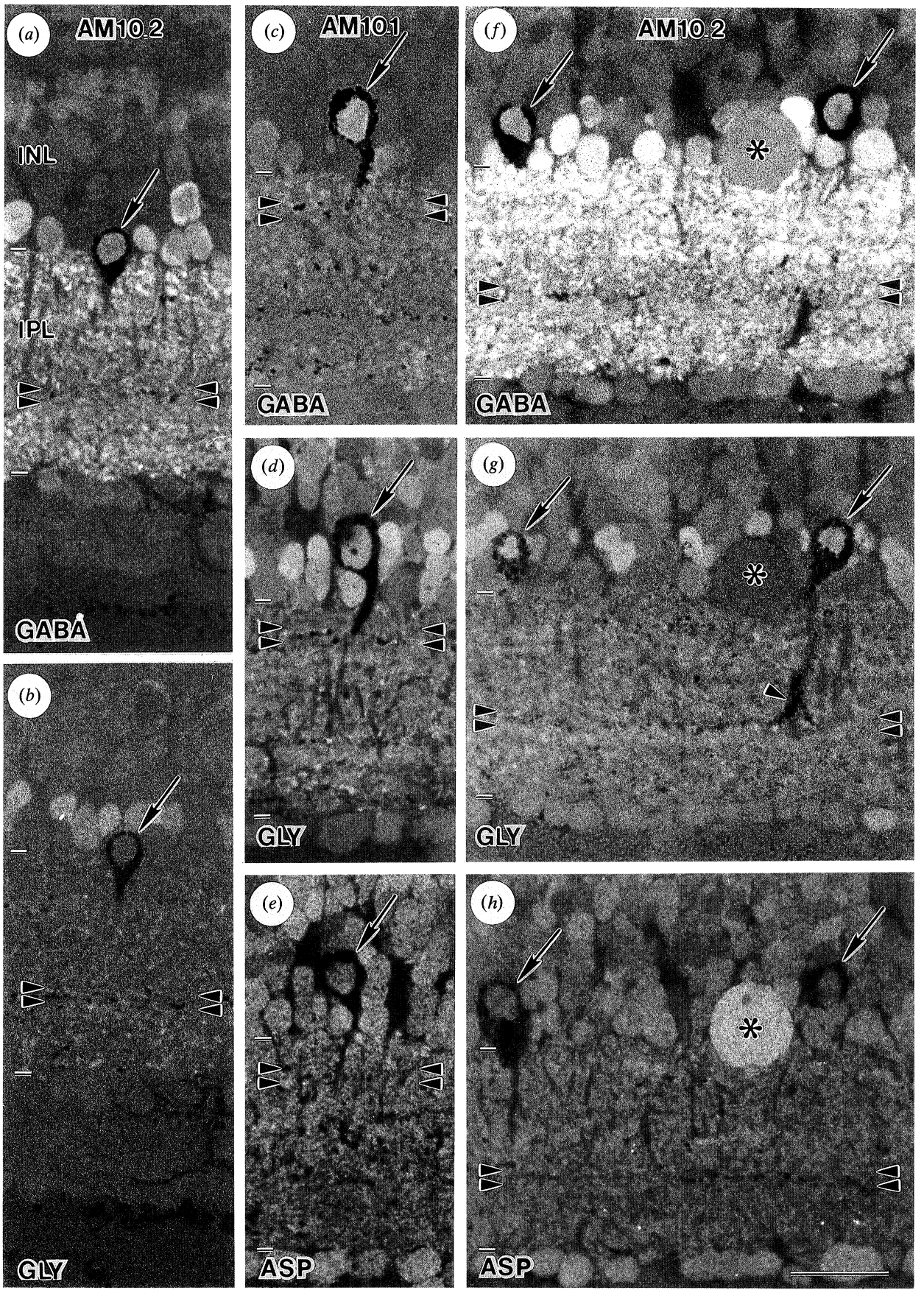

Figure 6. Neurochemical heterogeneity in AM10 cells demonstrated by postembedding immunocytochemistry on serial sections of Golgi-stained cells. Arrowheads in all micrographs show the ramification level of the Golgi-stained cells. (*a*,*b*) Serial sections of an AM10.2 cell (arrow) that contains GABA-IR (*a*), but not GLY-IR (*b*). (*c*–*e*) Serial sections of a Golgi-stained AM10.1 cell (arrow) reacted for GABA-IR (*c*), GLY-IR (*d*) and ASP-IR (*e*). The cell shows both GABA-IR and GLY-IR, but not ASP-IR. (*f*–*h*) Serial sections of two AM10.2 amacrine cells (arrows) reacted for GABA-IR (*f*), GLY-IR (*g*) and ASP-IR (*h*). A large spherical cell (asterisk) is present in all three micrographs and shows weak GABA-IR, no GLY-IR and strong ASP-IR, typical of this cell type (Sherry & Ulshafer 1992*b*). Calibration bar = 20 μm.

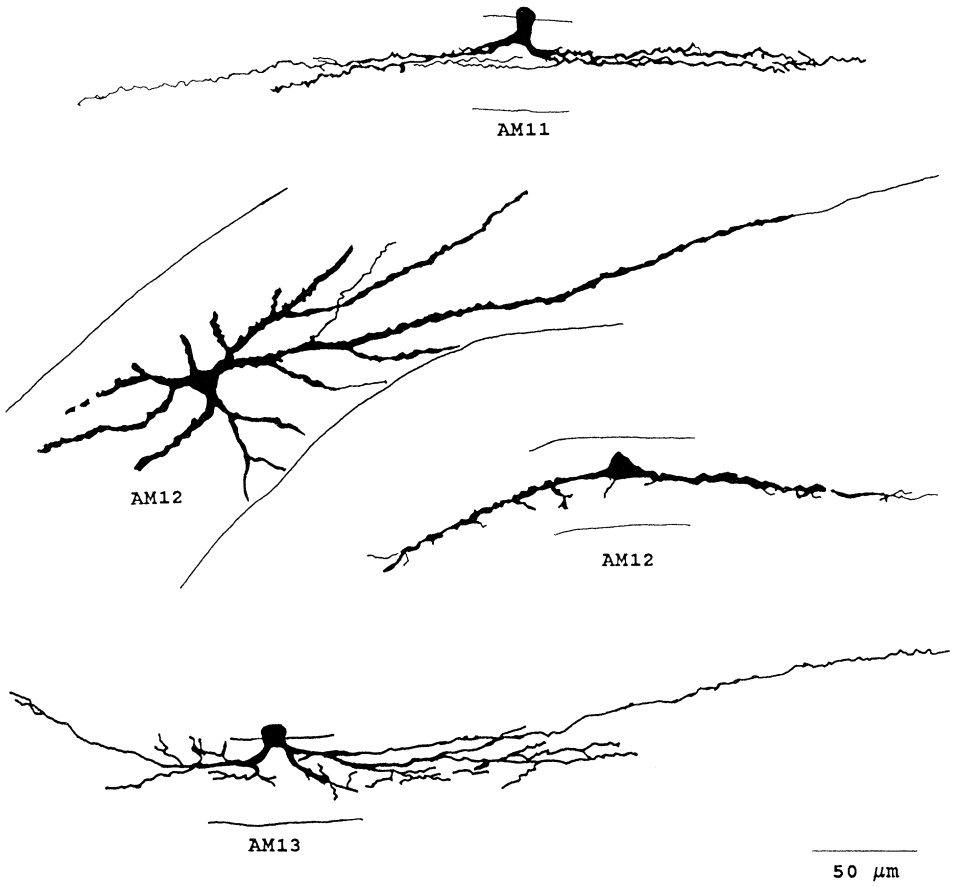

Figure 7. Camera lucida drawings of AM11, AM12 and AM13 cells. The AM12 cell on the left is oriented tangentially; the AM12 cell on the right is oriented radially. The AM13 cell shown is slightly oblique allowing visualization of the cell's planar dendritic arbor. All drawings to the same scale.

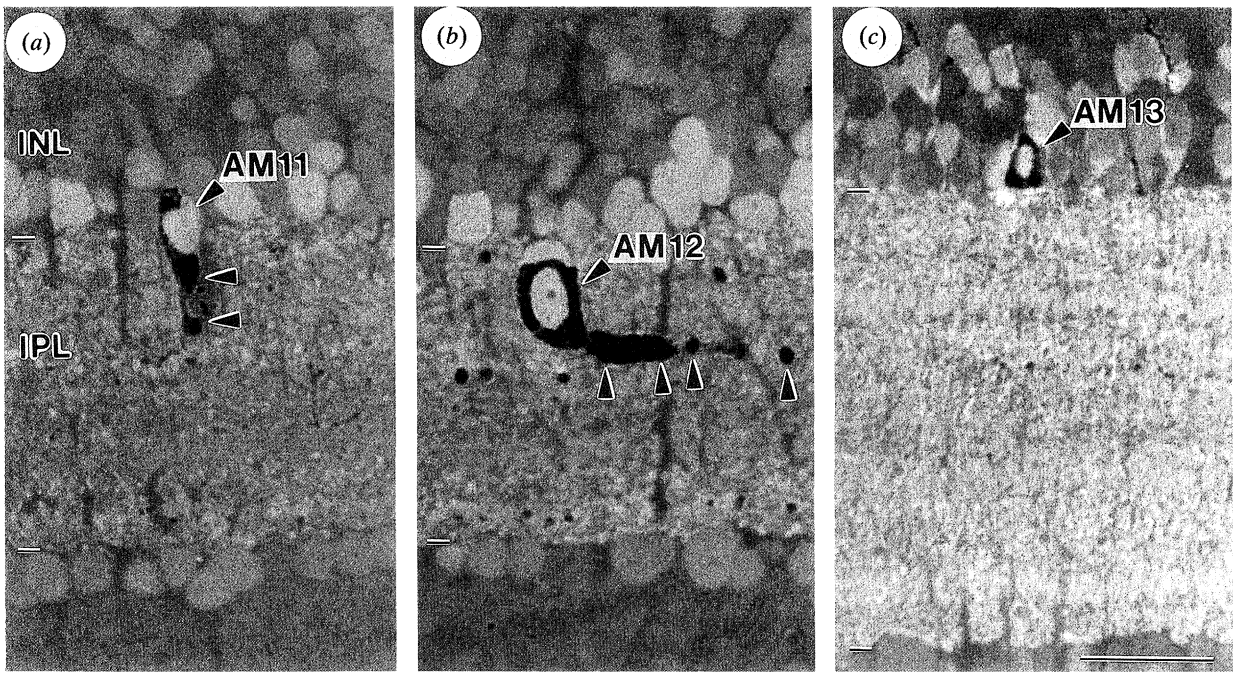

Figure 8. GABA-IR in AM11, AM12 and AM13 cells. (*a*) AM11 cell with an eccentrically placed, GABA-IR nucleus. Part of the descending process of this cell also is visible (arrowheads). (*b*) AM12 interstitial amacrine cell in the IPL. One of the cell's stout primary dendrites is present (arrowheads). (*c*) Example of a GABA-IR AM13 cell. Calibration bar = 20 μm.

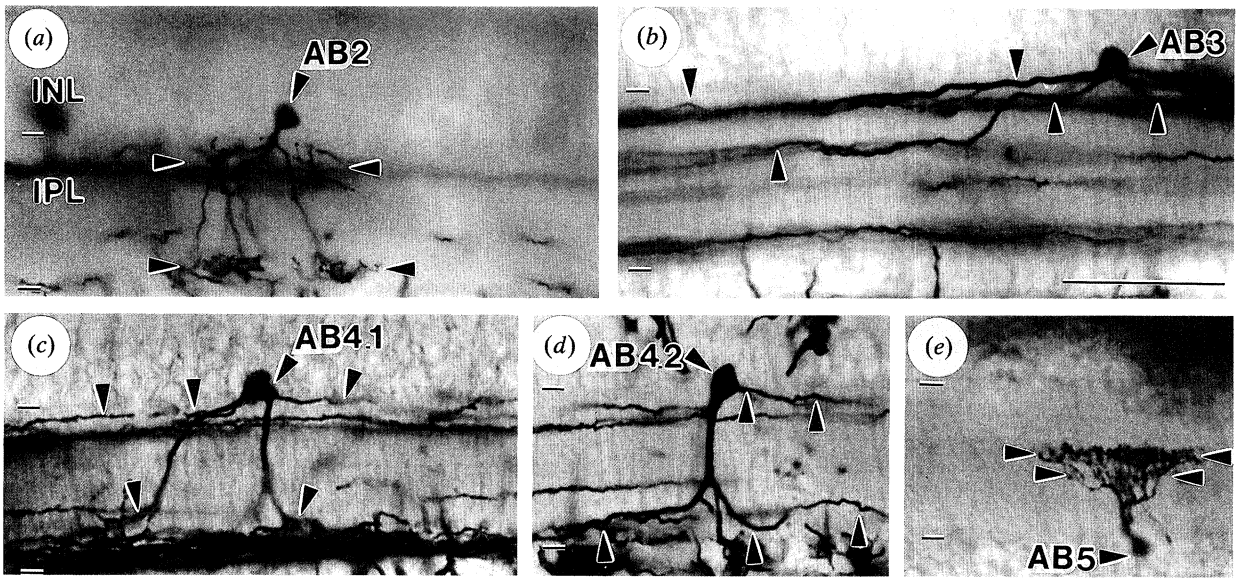

Figure 9. Golgi-stained bistratified amacrine cells. (*a*) AB2 cell with somewhat diffuse arborizations in the distal and proximal IPL (arrowheads). (*b*) AB3 cell stratifying in the distal and mid IPL (arrowheads). (*c*) AB4.1 amacrine cell with a multipolar soma and dendritic stratifications in the distal and proximal IPL (arrowheads). (*d*) AB4.2 cell. These cells are distinguished from AB4.1 cells by their pyriform soma, a single stout process descending to the proximal IPL, and a single process coursing in the distal IPL (all processes shown by arrowheads). Golgi-stained processes not marked with arrowheads arise from other impregnated cells nearby. (*e*) A displaced AB5 amacrine cell with a distinct stratum of boutons in the mid IPL and a smaller stratum of boutons at a more proximal depth in the IPL (arrowheads). Calibration bar = 50 μm.

in the most proximal INL and a small diameter dendritic field. The dendrites of this cell type were of medium thickness. Four of the five AB2 cells had a single primary dendrite but one cell had two primary dendrites. The AB2 cells had a loose stratum of dendrites in the distal IPL which gave rise to dendrites that descended into the proximal IPL and formed loose clusters of processes. Both cells tested showed GABA-IR (figure 11*a*) but not GLY-IR.

(iii) *Type AB3*

The AB3 cell type ($n = 6$; figures 9*b* and 10) was

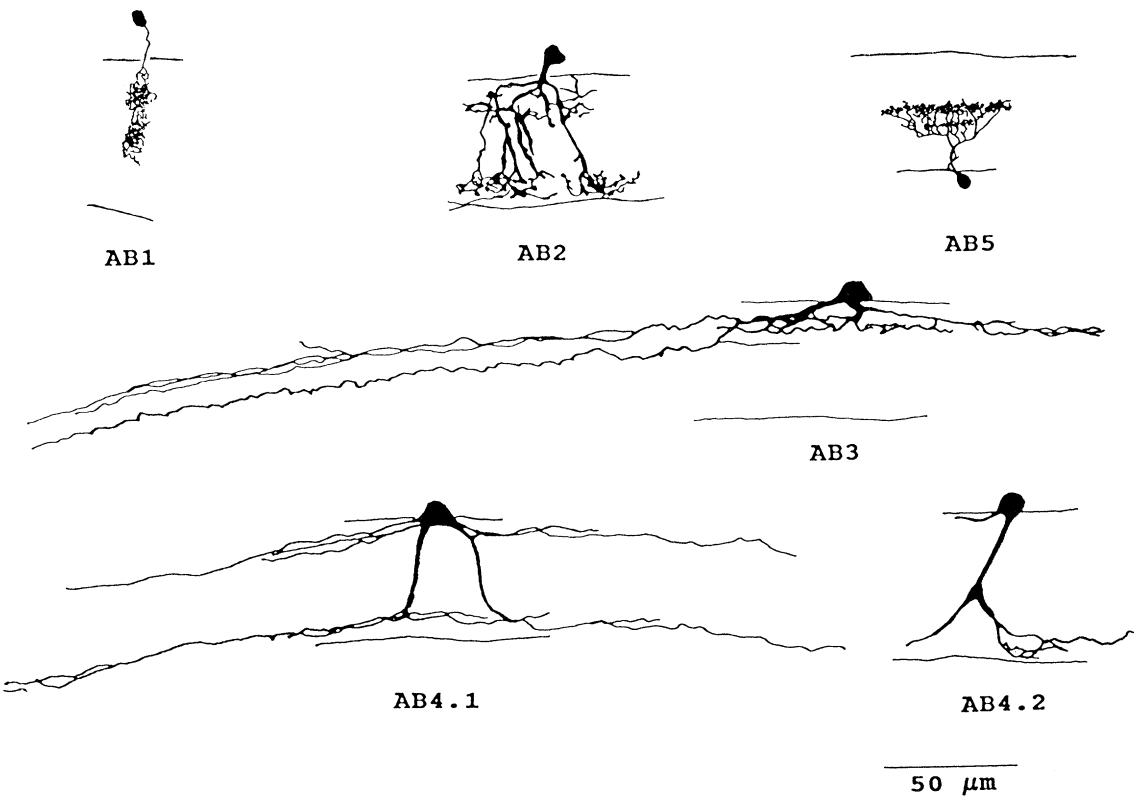

Figure 10. Camera lucida drawings of AB1, AB2, AB3, AB4.1, AB4.2 and AB5 cells. All cells drawn to same scale.

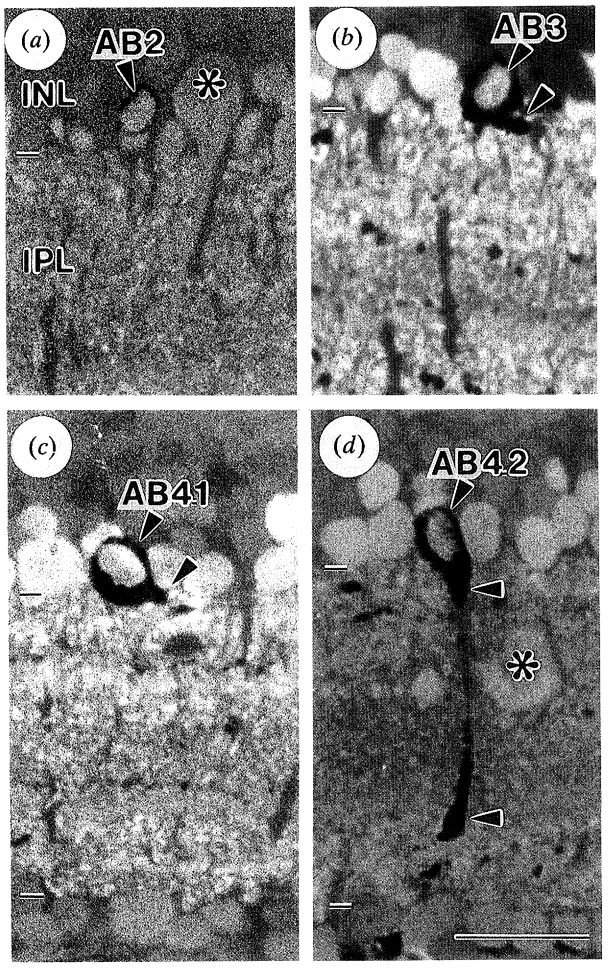

Figure 11. GABA-IR in Golgi-stained bistratified amacrine cells. (*a*) AB2 cell showing GABA-IR. A prominent non-impregnated amacrine cell showing GABA-IR (asterisk) is located nearby. (*b*) Intense GABA-IR in an AB3 cell. One of the primary dendrites can be seen leaving the soma (arrowhead). (*c*) Example of a GABA-IR AB4.1 cell showing a portion of one of the primary dendrites (arrowhead). (*d*) AB4.2 cell showing GABA-IR. The descending process of the cell is visible (arrowheads) and a non-impregnated, GABA-IR interstitial amacrine cell (asterisk) also is visible in the IPL. Calibration bar = 20 μm.

characterized by a rounded to fusiform multipolar soma located in the most proximal INL. There were two to four primary dendrites of medium diameter that gave rise to two relatively sparse strata of secondary dendrites; one in the distal IPL, one in the mid-IPL. These cells contained GABA-IR ($n = 2$; figure 11*b*), but not GLY-IR ($n = 1$).

(iv) *Type AB4*

The AB4 cell type was divided into two subtypes on the basis of somatic and dendritic differences. The AB4.1 subtype ($n = 4$; figures 9*c* and 10) was characterized by a rounded or fusiform multipolar soma in the proximal INL giving rise to two to four primary dendrites of medium thickness. The primary dendrites gave rise to sparse ramifications in the most distal or most proximal portions of the IPL. The AB4.1 dendritic field was symmetrically arranged and fell into the medium to wide field category. The two AB4.1 cells tested showed GABA-IR (figure 11*c*), but the AB4.1 cell tested for GLY-IR did not show labelling.

The AB4.2 subtype ($n = 3$; figures 9*d* and 10) was characterized by a pyriform soma in the proximal INL that gave rise to two primary dendrites of medium diameter. One dendrite originated from the proximal pole of the soma and descended directly to the innermost portion of the IPL where it gave rise to a sparse, symmetrical ramification of secondary dendrites. The other primary dendrite arose from the proximal side of the soma and ramified without branching, creating an asymmetrical field in the distal portion of the IPL. The dendritic fields of all AB4.2 cells were truncated by sectioning and dendritic field class was not determined. Both AB4.2 cells tested contained GABA-IR (figure 11*d*), but the one cell tested for GLY-IR did not show labelling.

(v) *Type AB5*

The AB5 cell type ($n = 1$; figures 9*e* and 10) was the only displaced amacrine cell type identified. The soma of this cell type was small and pyriform. The cell was a small field variety with slender dendrites that gave rise to two strata of boutons in the IPL. The most distal stratum of boutons had a considerably wider field diameter than the more proximal stratum. The cell did not show either GABA-IR or GLY-IR.

(*c*) *Tristratified amacrine cell types*

Tristratified amacrine cells ($n = 12$) were the least-frequently observed class of stratified amacrine cells. Tristratified cells comprised only two types.

(i) *Type AT1*

This striking cell type ($n = 11$; figures 12*a* and 13) was easily identified by its very narrow field, three characteristic strata of dense boutons and a few fine dendrites that descended into the most proximal IPL. We have termed these cells 'Medusa cells' because of their similarity in appearance to the medusa stage of jellyfish. Processes from other stratified cells often passed through the boutons. The average dendritic field diameter for this cell type was as follows: D1, 16.9 ± 5.1 μm; D2, 23.8 ± 5.4 μm; D3, 16.4 ± 2.7 μm. Several Golgi-stained AT1 cells were found in very close proximity to one another, but their dendritic fields did not overlap. The small pyriform somas of these cells were separated from the INL–IPL border by several layers of amacrine cell somas. Seven AT1 cells were tested for GABA-IR and GLY-IR, and all showed GLY-IR (figure 14*a*), but not GABA-IR.

(ii) *Type AT2*

A single example of this cell type was seen (figures 12*b* and 13). The cell had a rounded, multipolar soma located in the proximal INL. The dendrites of the AT2 cell were relatively thick and had a smooth appearance. The dendritic field of the AT2 cell was truncated, but a diameter of about 250 μm was measured, indicating that AT2 cells probably have a

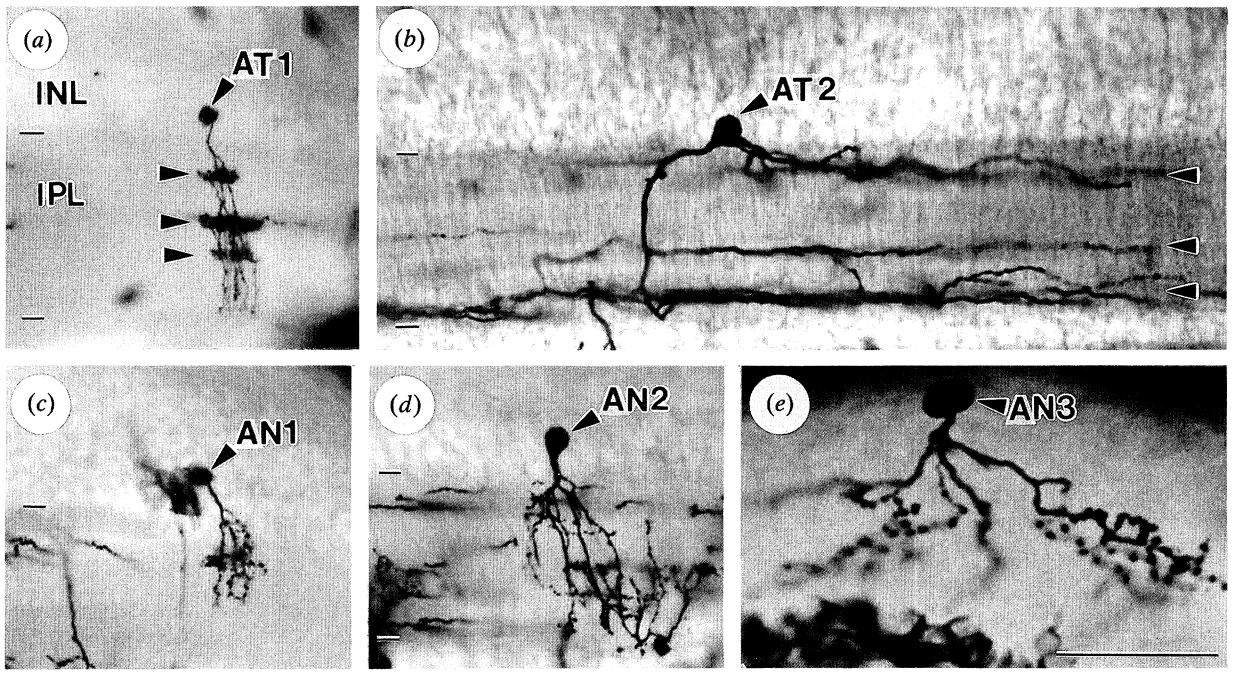

Figure 12. Golgi-stained tristratified and non-stratified cells. (*a*) A very narrow field 'Medusa' AT1 cell. The three tiers of boutons are clearly visible (arrowheads). (*b*) A multipolar tristratified AT2 cell. The three dendritic strata are shown with arrowheads. (*c*) Example of a very narrow field AN1 cell. The non-stratified dendrites of this cell type were restricted to the distal IPL and possessed many boutons. (*d*) A non-stratified AN2 cell with dendrites ramifying throughout the depth of the IPL. Processes from a Golgi-stained ganglion cell are visible in this micrograph, but close inspection showed no contact between the two cells. (*e*) Example of an AN3 amacrine cell characterized by large boutons along the dendrites and a narrow dendritic field in the distal IPL. Calibration bar = 50 μm.

medium to large dendritic field. This cell showed GABA-IR (figure 14*b*), but not GLY-IR.

(*d*) *Non-stratified cell types*

Non-stratified cells were characterized by dendritic arbors lacking a concentration of processes or boutons at any specific depth in the IPL, and are similar to 'diffuse' amacrine cells reported in other studies. Non-stratified cells were stained only rarely in our preparation ($n=9$) and comprised three types.

(i) *Type AN1*

Cells of the AN1 type ($n=4$; figures 12*c* and 13) were characterized by small, pyriform somas separated from the INL–IPL border by several layers of cell bodies. The dendrites of these cells were fine with a few boutons. The dendrites ramified in sublamina *a*

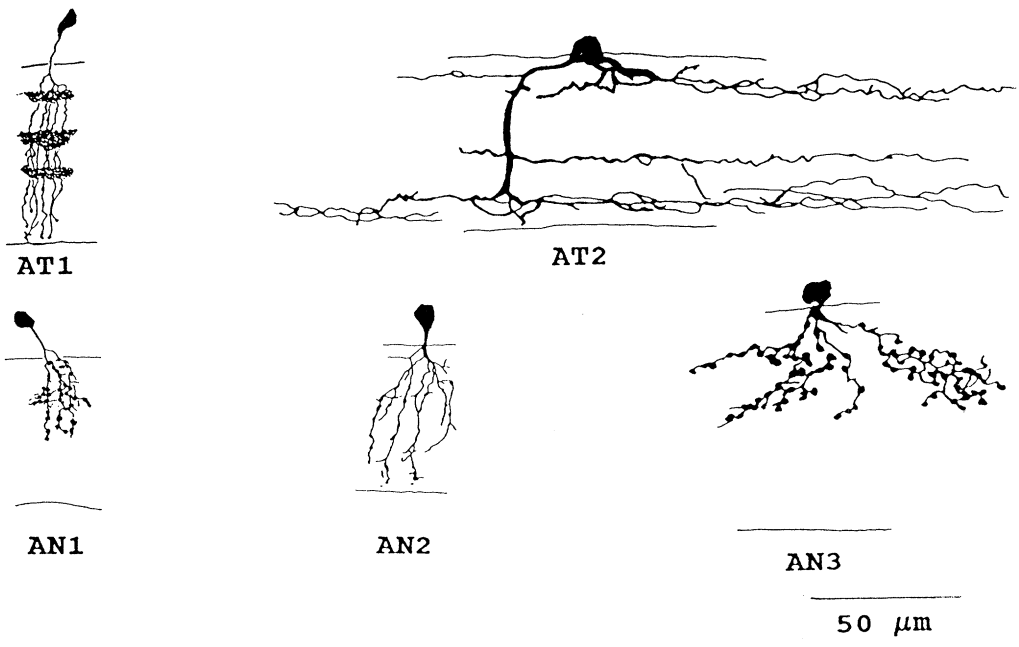

Figure 13. Camera lucida drawings of AT1, AT2, AN1, AN2 and AN3 cells. All cells drawn to same scale.

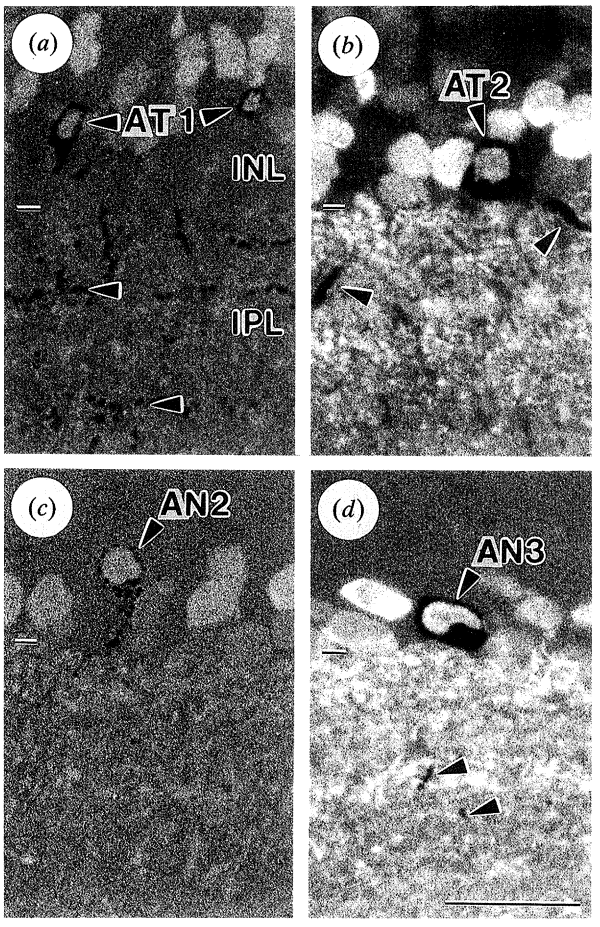

Figure 14. GLY-IR and GABA-IR in tristratified and non-stratified amacrine cells. (*a*) Two GLY-IR AT1 'Medusa' cells are present in the micrograph. Two tiers of boutons belonging to the cell on the left are visible in the IPL (arrowheads). (*b*) GABA-IR in the nucleus of the AT2 cell. Parts of the dendrites of this cell can be seen in the IPL (arrowheads). (*c*) GABA-IR in an AN2 cell. The Golgi deposits in this cell have a granular appearance. (*d*) Intense GABA-IR in an AN3 cell. Some boutons from this cell can be seen in the IPL (arrowheads). Calibration bar = 20 μm.

and formed a very narrow field (average dendritic field diameter = 21.6 ± 2.7 μm). The AN1 cell tested showed GLY-IR but not GABA-IR.

(ii) *Type AN2*

Cells of the AN2 cell type ($n = 2$; figures 12*d* and 13) had somatic and dendritic characteristics similar to AN1 cells described above, but the dendrites of AN2 cells spanned both sublaminae *a* and *b* of the IPL and had an average dendritic field diameter of 20.7 μm. Both cells showed GABA-IR (figure 14*c*) but not GLY-IR.

(iii) *Type AN3*

Cells of the AN3 cell type ($n = 3$; figures 12*e* and 13) had somas located near the INL–IPL border and were characterized by dendrites with clusters of boutons ramifying in sublamina *a*. The dendritic field fell into the narrow category (average dendritic field diameter = 75.1 ± 31.0 μm). The cell tested contained only GABA-IR (figure 14*d*).

(*e*) *Neurotransmitter-related enzyme localization*

Amacrine cell morphology and neurotransmitter content were investigated further by postembedding immunocytochemistry of neurotransmitter related enzymes in conventionally processed tissue. Colocalization of GABA and TOH, the rate limiting enzyme for catecholamine synthesis, was examined by serial section analysis of GABA-IR and TOH-IR. Localization of GAD, the synthetic enzyme for GABA, was examined immunocytochemically for comparison to GABA-IR.

(i) *TOH*

Both AB4 subtypes resemble cells that contain TOH-IR in the retina of the lizard *Uta stansburiana* with bistratified processes in the distal and proximal IPL (Engbretson & Battelle 1987). Localization of TOH-IR in conventionally processed *Anolis* retina showed TOH-IR in sparsely distributed amacrine cells resembling both Golgi-stained AB4 subtypes (figure 15*a*,*c*). Two strata of TOH-IR were seen in the IPL, one in the distal IPL and one in the proximal IPL, consistent with the localization of TOH to AB4 cells. Serial section analysis showed that all TOH-IR cells also contained GABA-IR of moderate intensity ($n = 6$; figure 15*b*,*d*), indicating the colocalization of GABA with a catecholamine, most likely dopamine, in AB4 cells. There was no evidence of TOH-IR interplexiform cells. A few TOH-IR processes arising from TOH-IR amacrine cells were seen ascending through the INL, but were never observed in the OPL as would be expected of an interplexiform cell process.

(ii) *GAD*

Localization of GAD-IR in the *Anolis* retina showed horizontal cells, cells in the ganglion cell layer, amacrine cells and a high degree of stratification in the IPL (figure 16). Amacrine cell bodies that showed GAD-IR were encountered less frequently than GABA-IR amacrine cell bodies, similar to several other species (see Yazulla 1991), including turtle (Hurd & Eldred 1989). The morphological characteristics of many GAD-IR amacrine cells were similar to GABA-IR cell types identified in Golgi-stained tissue, including cells that probably correspond to AM7, AM10, AM11 and AM12 cells (figure 16*a*–*d*, respectively). Multipolar cell bodies with GAD-IR that could correspond to AM13, AB3, AB4.2 and/or AT2 cells also were seen (figure 16*e*).

4. DISCUSSION

We have identified the morphology and neurotransmitter content of amacrine cells in the lizard retina, including 17 GABA-IR cell types, three GLY-IR cell types, and four amacrine cell types that did not contain either GABA-IR or GLY-IR (summarized in figure 17). The results reported here corroborate that *Anolis* GABA-IR and GLY-IR amacrine cells are largely exclusive populations (Sherry & Ulshafer 1992*a*; Sherry *et al.* 1993). Analysis of amacrine cell stratification patterns indicates that the GABA and

GLY amacrine cell types probably have diverse functional roles in visual processing.

A difficulty encountered in morphological studies is establishing classification criteria that distinguish cell types without introducing artificial distinctions. We classified the amacrine cells in this study on the bases of somatic and dendritic criteria. Our classification scheme stresses the dendritic features of the cell because these features are closely related to its functional organization (see reviews by Masland 1988; Wässle & Boycott 1991).

Neurotransmitter identification experiments confirmed that morphologically distinct cell types were also consistently neurochemically distinct (neurochemical heterogeneity in the AM10 cell type is considered below). Thus, the close correlation of morphology and neurotransmitter content common to many amacrine cells, such as cholinergic (Famiglietti 1983; Masland *et al.* 1984) or neuropeptide-containing cell types (cf. Eldred & Karten 1983), is also a property of *Anolis* GABA- and GLY-containing amacrine cell types. In addition, within the GABA- and GLY-containing amacrine cell types, each cell type shows a characteristic intensity level of immunoreactive labelling (Sherry and Ulshafer 1992*a*; Sherry *et al.* 1993). This was also the case for the Golgi impregnated cells. For example, the pyriform AM6 and AM7 cells contained intense GABA-IR; while AM9 cells, which are also monostratified pyriform cells and very similar in appearance to AM6 cells, showed relatively weak GABA-IR. Similarly, in cat retina, Pourcho (1980) reported that GABA- and GLY-accumulating amacrine cells could be differentiated not only on the basis of cytologic features but also on the density of ^{3}H-GABA and ^{3}H-glycine labelling.

(*a*) *Number and diversity of amacrine cell types*

Golgi staining is an effective method for visualizing the morphology of many amacrine cell types. Golgi staining has revealed 43 amacrine cell types in the fish retina (Wagner & Wagner 1988) and over twenty types in cat (Kolb *et al.* 1981), monkey (Boycott & Dowling 1969; Mariani 1990), human (Boycott & Dowling 1969; Kolb *et al.* 1992), turtle (Kolb 1982; Kolb *et al.* 1988) and now lizard retinas (this paper).

Comparison of *Anolis* amacrine cell morphology to the morphology of amacrine cells in the retinas of lizard and turtle species reveals a number of potential correspondences and differences (Ramon y Cajal 1933; Kolb 1982; see table 4). Ramon y Cajal (1933) described 16 Golgi-stained amacrine cell types in the retina of the green lizard *Lacerta viridis*, compared to the 23 types described in the present report. Each study reported that some cell types comprised subtypes of cells that ramified at several levels in the IPL. For simplicity, only the major types are indicated for comparison in table 4. The most obvious correspondence is that Golgi impregnation in both studies strongly favoured large amacrine cells with stratified dendrites and somas in the most proximal INL, which introduces a bias towards GABA-containing amacrine

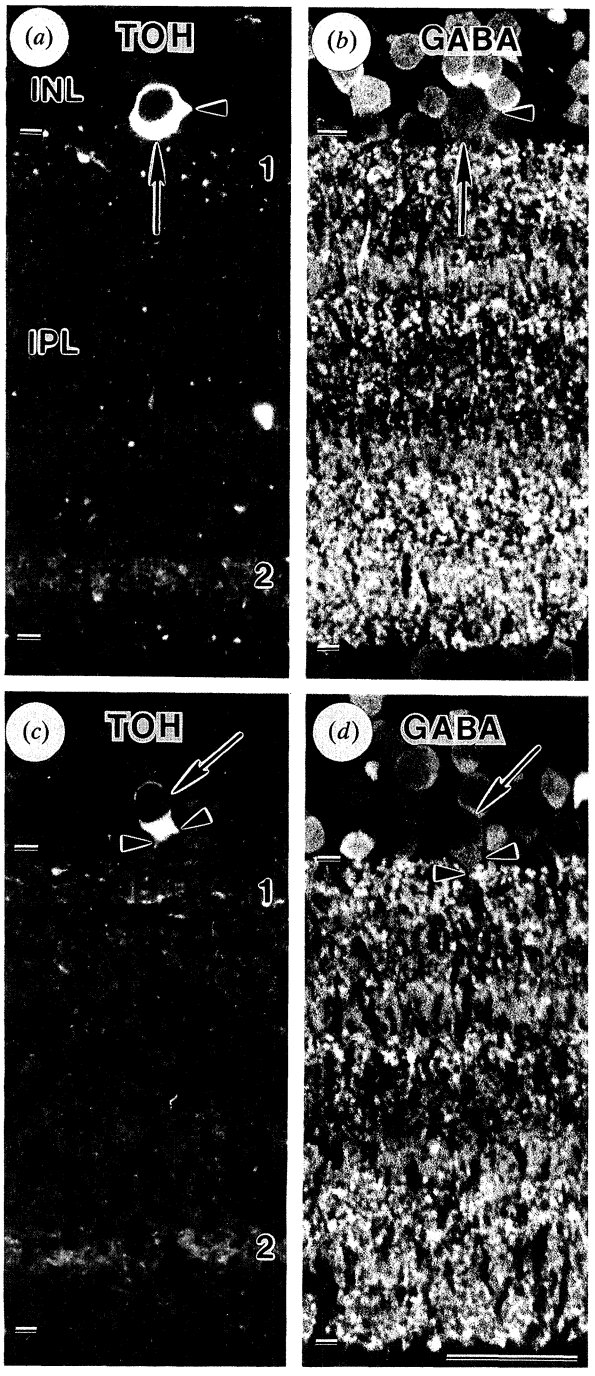

Figure 15. Serial section demonstration of TOH-IR and GABA-IR colocalization in AB4.1 (*a*,*b*) and AB4.2 (*c*,*d*) cells. (*a*,*b*) TOH-IR in an amacrine cell with AB4.1 characteristics (arrow in *a*). TOH-IR is present in two strata in the IPL (1,2) at depths similar to the stratification depth of AB4 cells. The same cell shows GABA-IR on a serial section (arrow in *b*). The arrowhead in both micrographs points to a protrusion on the cell body that may give rise to an ascending process. (*c*,*d*) TOH-IR in a pyriform amacrine cell with AB4.2 characteristics (arrow in *c*). Two protrusions that probably represent the origin of the primary dendrites are visible (arrowheads). Two TOH-IR strata are present in the IPL (1,2). The same cell seen in a serial section shows moderately intense GABA-IR (arrow in *d*). Calibration bar = 20 μm.

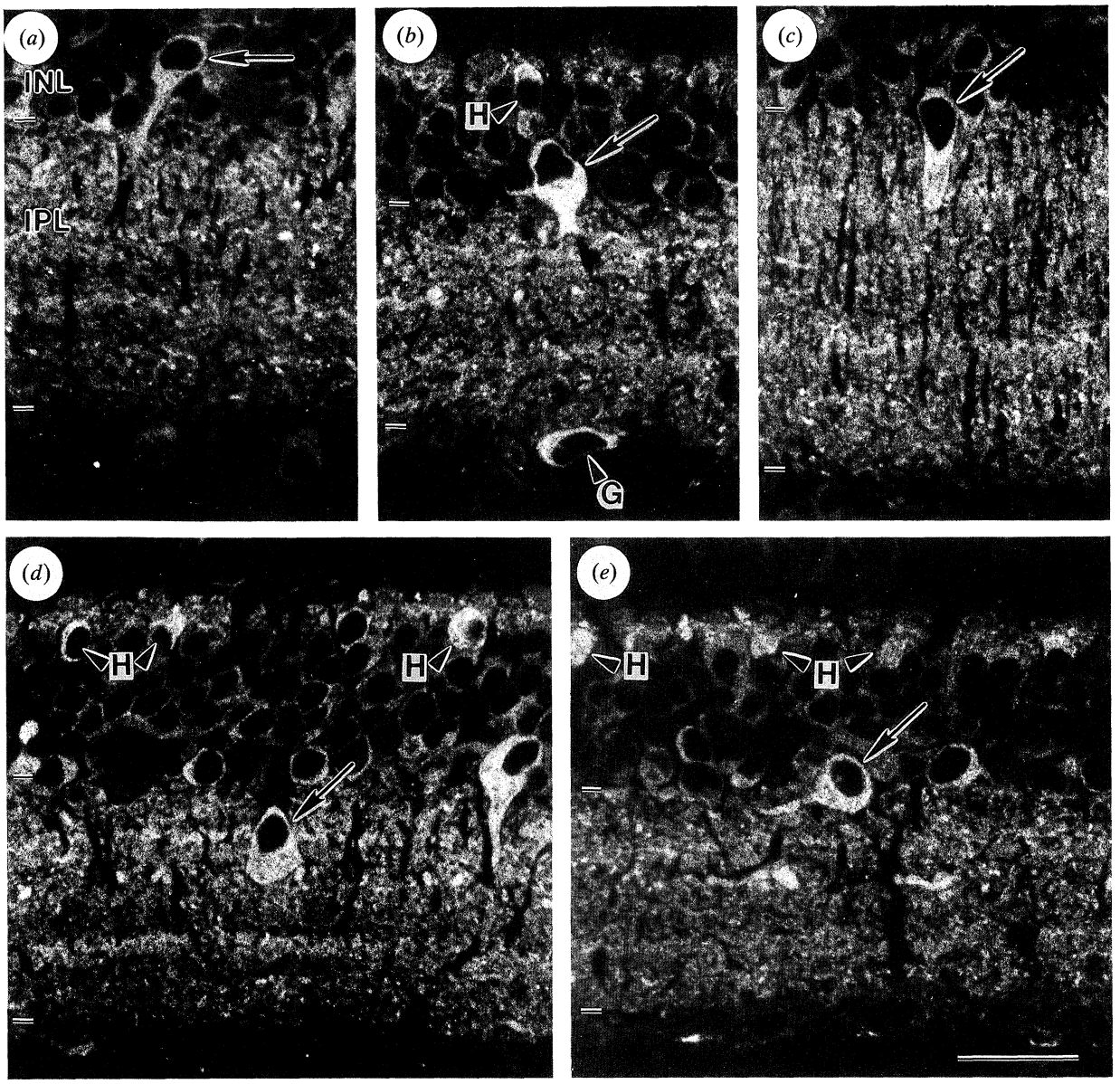

Figure 16. GAD-IR in the *Anolis* retina. GAD-IR is seen in horizontal and amacrine cells, cells in the ganglion cell layer and shows lamination in the IPL. (*a*) GAD-IR in a cell similar to an AM7 cell (arrow). (*b*) Intense GAD-IR in a large pyriform amacrine cell (arrow), similar in appearance to AM9 or AM10 cells. GAD-IR also is seen in a horizontal cell (H) and a cell in the ganglion cell layer (G). (*c*) GAD-IR in an amacrine cell (arrow) with the appearance of an AM11 cell. (*d*) GAD-IR in an interstitial amacrine (AM12) cell (arrow). Horizontal cells (H) and a large pyriform amacrine cell also show GAD-IR. (*e*) A multipolar amacrine cell showing GAD-IR (arrow) that could correspond to any of the AM13, AB3, AB4.1 or AT2 cell types. GAD-IR horizontal cells (H) and their processes also are present. Calibration bar = 20 μm.

cells rather than GLY-containing amacrine cells that have smaller, more distally placed somas (Sherry & Ulshafer 1992*a*; Sherry *et al.* 1993). A comparison reveals potential correspondence between 12 amacrine cell types (10 of which are monostratified) in the two lizard species (table 4), leaving 5 of Ramon y Cajal's cell types and 11 of our cell types without obvious counterparts. Note, types AM9 and AM10 cells may be accounted for by a single type of monostratified cell described by Ramon y Cajal (table 4). Both studies identified three non-stratified cell types but only one of these types, AN2, was identified in both studies. A major difference between the two studies is the number of multistratified cell types identified; Ramon y Cajal described a single bistratified cell type compared to five bistratified and two tristratified cell types in this study. Interstitial cells were absent in *Lacerta* but were present in *Anolis*. However, 'giant' amacrine cells were identified in *Lacerta* but not in *Anolis*. In summary, amacrine cells in the retinas of *Anolis* and *Lacerta* comprise similar morphological types and the discrepancies can be accounted for by differences in sampling by Golgi impregnation.

Estimating the total number of lizard amacrine cell types is difficult. Based on the similarity of *Lacerta* and *Anolis* amacrine cell populations, an estimate of 27 types is reached from Golgi studies (12 corresponding types and 15 types identified only in *Anolis* or *Lacerta*). It is clear from immunocytochemical studies in *Anolis* that even greater diversity in the amacrine cell

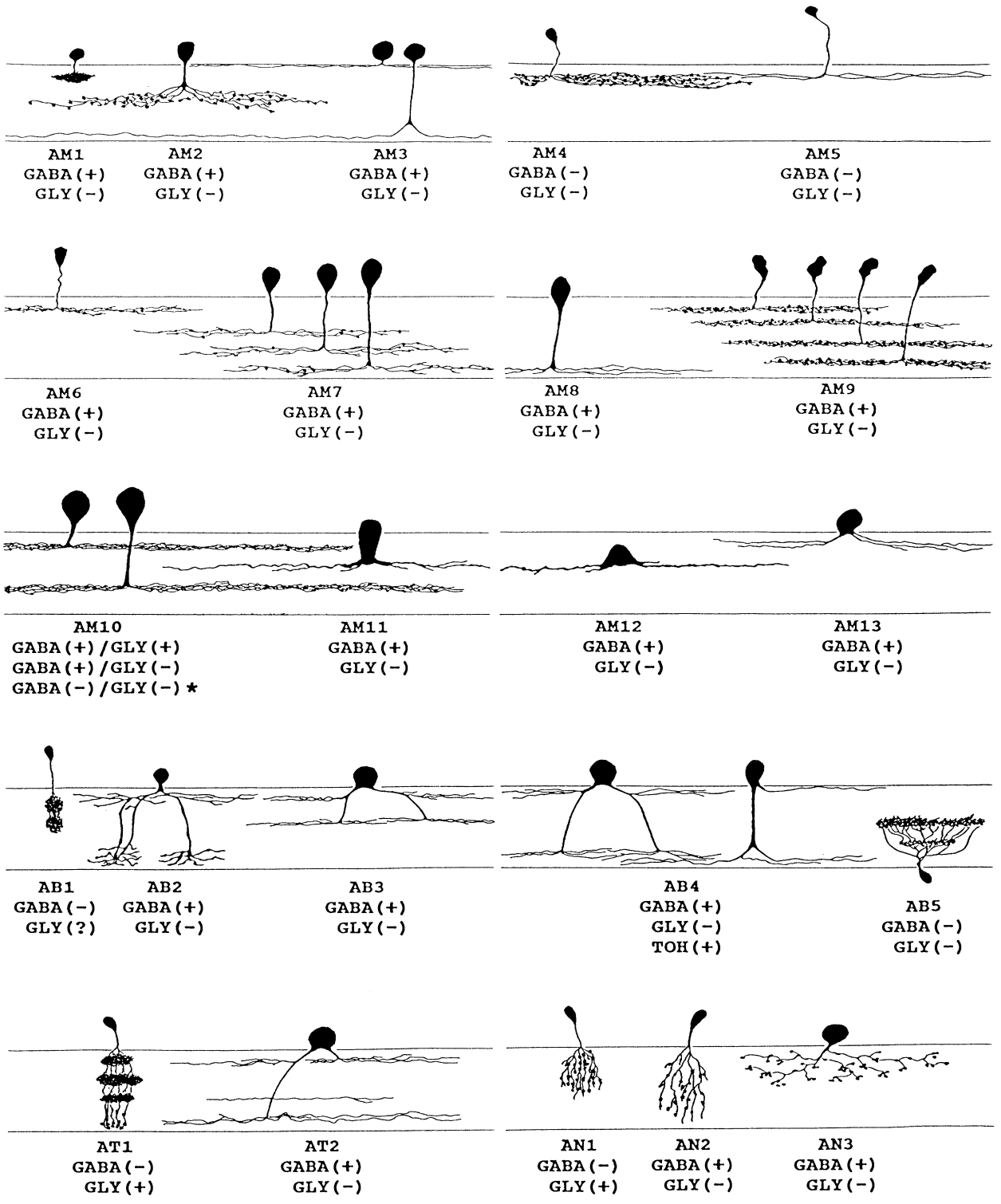

Figure 17. Summary diagram showing the morphology, stratification pattern and neurotransmitter content of Golgi-stained *Anolis* amacrine cells. Seventeen types contained GABA; three types contained GLY; and the neurotransmitter content of four amacrine cell types was not determined. No cells characterized in this study contained ASP. * The AM10 cell type had three neurochemical subtypes: Both AM10.1 and AM10.2 subtypes had GABA(+)-GLY(+) and GABA(+)-GLY(−) cells, but GABA(−)-GLY(−) cells were only observed within the AM10.1 subtype.

Table 4. *Potential correspondence of Golgi-stained* Anolis *amacrine cells with reptilian amacrine cells identified by Golgi staining or immunocytochemistry (ICC)*

Anolis Golgi type	*Anolis* ICC type[a]	*Lacerta* Golgi type[b]	*Psuedemys* Golgi type[c]
AM1	—	figure 5*c*?	A2?
AM2	—	figure 4*h*?	—
AM3.1	—	—	A17
AM3.2	A2	figure 5*d*?	A16
AM4	—	—	—
AM5	—	figure 5*h*?	—
AM6	A3	—	—
AM7.1	$A1_2$	—	—
AM7.2	$A1_2$	figure 4*d*	A25
AM7.3	$A1_2$	figure 4, no label	A26
AM8	$A1_1$	figure 4*c*	—
AM9.1	$A1_2$	figure 4*g*?	—
AM9.2	$A1_2$	figure 4*g*?	—
AM9.3	$A1_2$	figure 4*g*?	—
AM9.4	$A1_2$	figure 4*g*?	—
AM10.1	$A1_2$	figure 4*g*?	—
AM10.2	$A1_2$	figure 4*g*?	—
AM11	—	figure 4*e*?	—
AM12	INT 1	—	—
AM13	A4	figure 4*f*?	A18?
AB1	—	—	—
AB2	—	—	A11?
AB3	A4	—	A14?
AB4.1	A4	figure 5*g*	A15
AB4.2	—	—	—
AB5	—	—	—
AT1	—	—	—
AT2	A4	—	—
AN1	—	—	—
AN2	A2	figure 5*a*	A1
AN3	A5?	—	—

[a] Sherry & Ulshafer (1992*a*); lizard, *Anolis carolinensis*.
[b] Ramon Y Cajal (1933); lizard, *Lacerta viridis*.
[c] Kolb (1982); turtle, *Psuedemys scripta elegans*.

population is present. The current study does not account for the GABA-IR displaced amacrine cells, the distally placed multipolar cells (Sherry & Ulshafer 1992*a*) or either ASP-IR amacrine cell type (Sherry & Ulshafer 1992*b*). These results, taken together with the apparent bias against Golgi impregnation of GLY-IR amacrine cells, indicate that lizard amacrine cells encompass a very large number of cell types.

The seventeen types of GABA-IR amacrine cell characterized in this study showed greater morphological diversity than has been reported previously (see Pourcho & Goebel 1983; Hurd & Eldred 1989; Sherry & Ulshafer 1992*a*). Many studies of GABA-containing amacrine cells have used experimental approaches that may underestimate the actual number of GABA-containing cell types, since most techniques do not provide extensive visualization of the dendrites of single cells. A previous study of conventionally processed *Anolis* retina, relying primarily on somatic classification criteria, only identified six GABA-IR amacrine cell types (Sherry & Ulshafer 1992*a*). Some of the cell types identified previously include several Golgi-stained cell types (see table 4). For example, the $A1_2$ cell type (Sherry & Ulshafer 1992*a*) includes three Golgi-stained cell types identified in this study (AM7, AM9 and AM10).

The three types of GLY-IR amacrine cell showed less diversity than the GABA-IR cells. GLY-IR amacrine cells are slightly less numerous than GABA-IR amacrine cells (Sherry *et al.* 1993) and also may be less diverse. Fewer GLY-IR than GABA-IR amacrine cell types can be distinguished by conventional immunocytochemistry in *Anolis* (Sherry & Ulshafer 1992*a*; Sherry *et al.* 1993); and two of the GLY-IR cell types identified in this study have very narrow dendritic fields, which would require many cells of the same type to provide dendritic coverage of the IPL. *Anolis* GLY-IR amacrine cells tend to have small pyriform somas, located somewhat distally in the INL, and fine processes. However, Golgi staining in our preparation, as with Ramon y Cajal (1933), favoured labelling of cells with morphological properties of GABA-IR amacrine cells (see above), and some GLY-IR amacrine cell types probably have not been identified. Bias against identifying GLY-IR amacrine cell types also might be introduced if nuclear pools of GLY are particularly labile, which could cause a high false negative rate. False negative results could account for the absence of GLY-IR in cells with GLY-related morphological features, such as AM4 and AM5 cells, but this seems unlikely considering the reliability of demonstrating GLY-IR in other amacrine cell types.

ASP-IR amacrine cells, which comprise at least two types in *Anolis* (Sherry & Ulshafer 1992*b*), were absent from our sample of Golgi-stained cells. No Golgi-stained cells resembling the large spherical ASP-IR cells of the *Anolis* retina (Sherry & Ulshafer 1992*b*) were seen, although non-Golgi-stained cells of this type were observed (see figure 6*h*). Ramon y Cajal (1933) reported that a giant amacrine cell with a semilunar soma in lizard retina was refractory to Golgi impregnation but could be observed with Dogiel's method (Ramon y Cajal 1933, Plate III, figure 7*n*). Large diameter dendrites arose from opposite sides of the soma and were restricted to sublamina *a*. Considering their comparably large, round soma and their apparent refractoriness to Golgi impregnation, we suggest that this giant amacrine cell of the second layer corresponds to the large ASP-IR amacrine cell type in lizard retina.

Four amacrine cell types were neither GABA-IR nor GLY-IR. Considering that up to 80% of amacrine cells contain either GABA or GLY, at least 20% of the amacrine cell population can be expected to contain neither GABA nor GLY (Marc 1985; Yazulla 1986). The neurotransmitter of the non-GABA-IR-GLY-IR cell types is not known, but there are many candidates among the classical and neuropeptide neurotransmitters that have been localized to amacrine cells (see Brecha 1983).

(*b*) *Neurochemical heterogeneity within a cell type*

The AM10 cell type contained three neurochemical classes (GABA-IR only, GABA-IR plus GLY-IR, no

GABA-IR or GLY-IR). These results are consistent with immunocytochemical labelling of type $A1_2$ amacrine cells in conventionally processed tissue. Two neurochemical classes of *Anolis* $A1_2$ amacrine cells were identified: cells that colocalize GABA-IR and GLY-IR, and cells that contain GABA-IR only (Sherry *et al.* 1993), similar to two of the three neurochemical subtypes of AM10 cells. The morphological characteristics of the three neurochemical classes of AM10 cell appear identical in radial sections, but cells that appear similar in radial section may have very different dendritic organization when viewed tangentially (cf. Wagner & Wagner 1988), and the possibility that AM10 cells comprise more than one cell type must be considered. The functional ramifications of neurochemical heterogeneity within a morphological cell type are not clear. One obvious question is whether the synaptic organization of the different neurochemical types of AM10 cells differ, which would indicate functional heterogeneity as well.

(*c*) *Functional organization of amacrine cells*

Amacrine cell physiology in retinas of non-mammals is highly correlated with cell morphology and dendritic organization in the IPL and several general organizational patterns have emerged (Famiglietti *et al.* 1977; Teranishi *et al.* 1987; Ammermüller & Weiler 1989; Djamgoz *et al.* 1990; Yang *et al.* 1991). However, it must be stressed that several exceptions to these rules have been described, particularly in turtle retina (Ammermüller & Weiler 1989). Monostratified cell types often have sustained ON or OFF responses according to the cell's ramification in either sublamina *b* or *a* of the IPL, respectively. Multistratified and non-stratified cell types often have transient responses, with narrow field cells showing faster characteristics than wide field cells. Amacrine cell types with highly polarized dendritic fields may possess complex physiological responses like colour-coding or direction selectivity (Djamgoz *et al.* 1990; Naka 1980). Each morphologically distinct amacrine cell type appears to be physiologically unique (Ammermüller & Weiler 1989).

Despite anatomical differences in the organization of the GABA and GLY systems in the *Anolis* IPL (Sherry *et al.* 1993), segregation of GABA and GLY into different amacrine cell types (Sherry *et al.* 1993; this paper), and the correlation of amacrine cell morphology and physiology, no simple functional organization of the GABA and GLY systems in the *Anolis* IPL is obvious. For example, both GABA and GLY are probably involved in both sustained and transient circuits because both neurotransmitters were localized to monostratified and multistratified cell types, similar to salamander retina in which GABA and GLY are associated with both sustained and transient amacrine cell types (Yang *et al.* 1991).

(*d*) *Stratification in the IPL*

The anatomical and functional stratification of the IPL are closely related. The functional division of the IPL into OFF and ON sublaminae (sublamina *a* and *b*, respectively) is well known (cf. Famiglietti & Kolb 1976; Famiglietti *et al.* 1977; Teranishi *et al.* 1987; Ammermüller & Weiler 1989). However, within each of the broad sublaminae *a* and *b*, it is clear that further substratification is present (cf. Ramon y Cajal 1933; Kolb 1982). In the *Anolis* retina, it is clear that the dendritic arbor of each cell type has a characteristic depth and extent in the IPL that will contribute to the substratification of the IPL. For example, *Anolis* AM4 and AM5 cells both ramify at about the same depth in the distal IPL. However, the AM4 cell is more broadly stratified than the AM5 cell and presumably differs in synaptic connectivity.

Substratification in the IPL is indicated further by the extensive lamination of GABA- and GLY-labelled processes, a feature particularly prominent in the retinas of frogs, reptiles and birds (reviewed by Marc 1986; Hurd & Eldred 1989; Sherry *et al.* 1993). There are four GABA-IR and seven GLY-IR strata in the *Anolis* IPL (Sherry *et al.* 1993). The peak densities of the GABA-IR strata interlace those of GLY-IR throughout the IPL in the parafovea and in the distal two-thirds of the IPL in the peripheral retina. Thus, even though the dendrites of GABA-IR and GLY-IR Golgi-stained cells are broadly distributed in the IPL strata, their dendritic distribution must be related to the complex substratification of GABA and glycine in the IPL indicating that the two systems interact with different targets and play different roles in retinal coding (Sherry *et al.* 1993).

Anatomically similar amacrine cells that ramify at different depths of the IPL may have analogous functions in parallel pathways within the IPL, i.e. ON versus OFF (see Marc 1989). The classic example of ON–OFF symmetry in amacrine cells is the mammalian cholinergic starburst amacrine cell (Famiglietti 1983; Masland *et al.* 1984). Similarly in *Anolis* three of the monostratified cell types may consist of two or more physiologically complementary ON and OFF subtypes (AM3, AM9, AM10). Ramon y Cajal (1933, Plate III, figure 4*a*) described a diffuse cell with dendrites concentrated in sublamina *b* that could complement the AN1 cell that ramifies in sublamina *a*. Anatomical and functional symmetry within the IPL appears to be a common feature in the vertebrate retina including bipolar cells (Famiglietti *et al.* 1977; Stell *et al.* 1977; Hare *et al.* 1986; Boycott & Wässle 1991; Sherry & Yazulla 1993*a*), amacrine cells (Famiglietti *et al.* 1977; Kolb 1982; Teranishi *et al.* 1987; Wagner & Wagner 1988; Kolb *et al.* 1988; Mariani 1990) and ganglion cells (Famiglietti & Kolb 1976; Famiglietti *et al.* 1977; Vallerga & Usai 1986) in a variety of species.

(*e*) *Comparative neurochemical morphology*

A large, pyriform amacrine cell type that ramifies in the most proximal IPL and exhibits GABAergic markers similar to the *Anolis* AM8 cell type is present turtle retina (Hurd & Eldred 1989). The GABA-IR lamination in turtle IPL (Hurd & Eldred 1989) is very similar to that observed in lizard retina and, as

we found in lizard, it is likely that there are multiple types of monostratified GABA-IR amacrine cells in turtle retina. Multiplicity of GABAergic monostratified pyriform amacrine cells also has been reported in goldfish and salamander retinas (Marc 1989; Yang *et al.* 1991) and appears to be a general feature of non-mammalian retinas.

Interstitial amacrine cells are a common feature of vertebrate retinas (Ramon y Cajal 1933). The GABA-IR AM12 cell appears to be the only interstitial cell type in the *Anolis* retina (Sherry & Ulshafer 1992*a*; Sherry *et al.* 1993; this paper), but other species (e.g. ox, roach) have multiple interstitial cell types (Ramon y Cajal 1933; Wagner & Wagner 1988) including both GABA-IR and GLY-IR types in goldfish (Yazulla & Studholme 1990). Turtle retina contains a neurotensin-IR interstitial cell type (Weiler & Ball 1984) but apparently none that are GABA-IR (Hurd & Eldred 1989), in contrast to lizard. Interstitial amacrine cells may serve a complementary physiological role (ON versus OFF) with morphologically similar orthotopic amacrine cells that ramify at a different IPL depth as suggested in fish (Teranishi & Negishi 1991). Alternatively, interstitial amacrine cells may ramify at the same level in the IPL as orthotopic amacrine cells of the same neurochemical type, as shown for TOH-IR amacrine cells in two species of bat (Studholme *et al.* 1987). Although interstitial amacrine cells are a common morphological feature in the retina, no common function for them among species is apparent.

The family of very narrow field cells with tiers of boutons (AM1, AB1, AT1) in the *Anolis* retina are neurochemically heterogeneous: with GABA-IR AM1 cells, GLY-IR AT1 cells and uncertain AB1 cells. Frog, turtle and chicken have amacrine cells that appear analogous to the *Anolis* AM1 cell (Ramon y Cajal 1933; Kolb 1982). However, cells analogous to the AB1 and AT1 cell types have not been described previously in any species, to our knowledge. The GLY-IR AT1 Medusa cells are particularly striking. Of all cell types with distally-placed somas in the INL, they were observed most frequently. Given their very narrow field, GLY-IR Medusa cells must be very numerous (at least 1600 per square millimetre) to provide complete retinal coverage. Of all cell types reported here, the synaptic organization of the individual tiers of AT1 Medusa cells may prove to be the most interesting and complex.

Amacrine cells that contain TOH are ubiquitous and generally thought to contain dopamine (cf. Wulle & Wagner 1990). The TOH-IR amacrine cells of the turtle retina are tristratified (Witkovsky *et al.* 1984; Kolb *et al.* 1987) whereas TOH-IR cells of the lizard retina are bistratified (Engbretson & Battelle 1987; this paper) and most closely match the morphology of the *Anolis* GABA-IR AB4 cell type. Our finding of colocalization of GABA-IR and TOH-IR in the presumptive AB4 cells is consistent with the results of Wulle & Wagner (1990) who reported such colocalization in retinas of amniote vertebrates, but not for amphibians and fish. The AB4 cells provide another example of substratification within a neurochemical class. The proximal arbor of AB4.1 cells ramifies slightly distal to the proximal arbor of AB4.2 cells even though both cells ramify in the most proximal 20% of the IPL.

Serotonin has been localized to tristratified amacrine cells similar to the GABA-IR *Anolis* AT2 cell in the retina of the lizard *Uta stansburiana* (Engbretson & Battelle 1987). Colocalization of serotonin-IR and GABA-IR has been reported in retinal amacrine cells in cat, salamander and rabbit (Wässle & Chun 1988; Watt 1992; Massey *et al.* 1992) and it is possible the *Anolis* AT2 cell type also contains serotonin in addition to GABA. There is variability in serotonin localization in retinas among reptilian species. For example, Lacertilian lizards contain monostratified serotonin-containing amacrine cells (Osborne 1984), and turtle retina (Weiler & Schütte 1985) contains at least two serotonin-accumulating amacrine cell types.

The neuropeptides enkephalin and substance P have been reported in *Anolis* retina (Brecha 1983; Brecha *et al.* 1984), but only substance P has been localized. Substance P in the *Anolis* retina is found in a pyriform amacrine cell type that ramifies broadly in the mid IPL (Brecha *et al.* 1984) and appears similar to the GABA-IR AM2 cell. The *Anolis* retina differs from the retinas of two Australian lizard species, (*Pogona vitticeps* and *Varanus gouldii*; Hiscock & Straznicky 1991) which contain two substance P-IR amacrine cell types. One cell type appears similar to the pyriform cell in *Anolis*, but the other cell type is a multipolar cell ramifying in the distal IPL and is apparently absent in *Anolis*. GABA and substance P colocalize in monostratified and bistratified amacrine cell types in cat retina (Pourcho & Goebel 1988) and may co-localize in lizard retina as well.

It seems reasonable to assume that, within a class of neuron, morphological differences will be reflected in differences in synaptic organization and hence in function. Amacrine cells are the most diverse retinal neurons in form as well in the variety of neurotransmitters proposed for their use. An important step in understanding this diversity is to assign particular neurotransmitters to each cell type. We have identified seventeen types of amacrine cell that are GABA-IR and three types that are GLY-IR, including one type in which these transmitters co-localize. It is not known why so many GABAergic amacrine cell types are needed. One possibility is that spatial and temporal tuning of each of the parallel chromatic channels involve separate sets of GABAergic amacrine cells. Regardless of the explanation, it is clear that one must describe GABA and glycine connectivity in the inner retina with regard for the morphological subtype of amacrine cell involved, as has been done for the scotopic pathway in cat retina (cf. Kolb & Nelson 1984) and rabbit retina (Strettoi *et al.* 1990, 1992), if we are to understand the neural organization of the retina.

This work was supported by a postdoctoral fellowship to D.M.S. (F32 EY06240) and a grant to S.Y. (RO1 EY01682). We thank Dr R. Wenthold, Dr J.-Y. Wu and Dr T. Joh for the gifts of their antisera.

REFERENCES

Ammermüller, J. & Weiler, R. 1989 Correlation between electrophysiological responses and morphological classes of turtle retinal amacrine cells. In *Neurobiology of the inner retina* (ed. R. Weiler & N. N. Osborne), pp. 117–132. Berlin: Springer-Verlag.

Boycott, B.B. & Dowling, J.E. 1969 Organization of the primate retina. *Phil. Trans. R. Soc. Lond.* B **255**, 109–176.

Boycott, B.B. & Wässle, H. 1991 Morphological classification of bipolar cells of the primate retina. *Eur. J. Neurosci.* **3**, 1069–1088.

Brecha, N. 1983 Neurotransmitters: histochemical and biochemical studies. In *Chemical neuroanatomy* (ed. P. C. Emson), pp. 85–129. New York: Raven Press.

Brecha, N.C., Eldred, W.D., Kuljis, R.O. & Karten, H.J. 1984 Identification and localization of biologically active peptides in the vertebrate retina. *Prog. Retinal Res.* **3**, 185–226.

Crescitelli, F. 1972 The visual cells and visual pigments of the vertebrate eye. In *Handbook of sensory physiology*, vol. VII/1 (ed. H. J. A. Dartnall), pp. 245–363. New York: Springer-Verlag.

Davanger, S., Ottersen, O.P. & Storm-Mathisen, J. 1991 Glutamate, GABA, and glycine in the human retina: an immunocytochemical investigation. *J. comp. Neurol.* **311**, 483–494.

Djamgoz, M.B.A., Spadavecchia, L., Usai, C. & Vallerga, S. 1990 Variability of light-evoked response pattern and morphological characterization of amacrine cells in goldfish retina. *J. comp. Neurol.* **301**, 171–190.

Dowling, J.E. 1968 Synaptic organization of the frog retina: an electron microscopic analysis comparing the retinas of frogs and primates. *Proc. R. Soc. Lond.* B **170**, 205–228.

Dowling, J.E. & Boycott, B.B. 1966 Organization of the primate retina: electron microscopy. *Proc. R. Soc. Lond.* B **166**, 80–111.

Eldred, W.D. & Cheung, K. 1989 Immunocytochemical localization of glycine in the retina of the turtle (*Pseudemys scripta*). *Visual Neurosci.* **2**, 331–338.

Eldred, W.D. & Karten, H.J. 1983 Characterization and quantification of peptidergic amacrine cells in the turtle retina: enkephalin, neurotensin and glucagon. *J. comp. Neurol.* **221**, 371–381.

Engbretson, G.A. & Battelle, B. 1987 Serotonin and dopamine in the retina of a lizard. *J. comp. Neurol.* **257**, 140–147.

Famiglietti, E.V.Jr, Kaneko, A. & Tachibana, M. 1977 Neuronal architecture of on and off pathways to ganglion cells in carp retina. *Science, Wash.* **198**, 1267–1269.

Famiglietti, E.V.Jr 1983 'Starburst' amacrine cells and cholinergic neurons: mirror-symmetric ON and OFF amacrine cells of rabbit retina. *Brain Res.* **261**, 138–143.

Famiglietti, E.V. & Kolb, H. 1976 Structural basis for ON- and OFF-center responses in retinal ganglion cells. *Science, Wash.* **194**, 193–195.

Hare, W.A., Lowe, J.S. & Owen, G. 1986 Morphology of physiologically identified bipolar cells in the retina of the tiger salamander, *Ambystoma tigrinum*. *J. comp. Neurol.* **252**, 130–138.

Hiscock, J. & Straznicky, C. 1991 Substance P-immunoreactive neurons in the retina of two lizards. *Arch. Histol. Cytol.* **54**, 321–337.

Hodgekinson, P.E. & Still, A.W. 1980 Color and brightness preferences in the lizard *Anolis carolinensis*. *Perception* **9**, 61–68.

Hurd, L.B.II & Eldred, W.D. 1989 Localization of GABA- and GAD-like immunoreactivity in the turtle retina. *Visual Neurosci.* **3**, 9–20.

Joh, T.H., Geghman, C. & Reis, D. 1973 Imunocytochemical demonstration of increased accumulation of tyrosine hydroxylase protein in sympathetic ganglia and adrenal medulla elicited by reserpine. *Proc. natn. Acad. Sci. U.S.A.* **70**, 2767–2771.

Kolb, H., Nelson, R. & Mariani, A. 1981 Amacrine cells, bipolar cells and ganglion cells in the cat retina: A Golgi study. *Vision Res.* **21**, 1081–1114.

Kolb, H. 1982 The morphology of the bipolar cells, amacrine cells and ganglion cells in the retina of the turtle *Pseudemys scripta elegans*. *Phil. Trans. R. Soc. Lond.* B **298**, 355–393.

Kolb, H., Cline, C., Wang, H.H. & Brecha, N. 1987 Distribution and morphology of dopaminergic amacrine cells in the retina of the turtle (*Pseudemys scripta elegans*). *J. Neurocytol.* **16**, 577–588.

Kolb, H., Perlman, I. & Normann, R.A. 1988 Neural organization of the retina of the turtle *Mauremys caspica*: a light microscope and Golgi study. *Visual Neurosci.* **1**, 47–72.

Kolb, H., Linberg, K.A. & Fisher, S.K. 1992 Neurons of the human retina: a Golgi study. *J. comp. Neurol.* **318**, 147–187.

Kolb, H. & Nelson, R. 1984 Neural architecture of the cat retina. *Prog. Retinal Res.* **3**, 21–60.

Makaretz, M. & Levine, R.L. 1980 A light microscopic study of the bifoveate retina in the lizard *Anolis carolinensis*: general observations and convergence ratios. *Vision Res.* **20**, 679–686.

Marc, R.E. 1985 The role of glycine in retinal circuitry. In *Retinal transmitters and modulators: models for the brain*, vol. 1 (ed. W. W. Morgan), pp. 119–158. Boca Raton, Florida: CRC Press.

Marc, R.E. 1986 Neurochemical stratification in the inner plexiform layer of the vertebrate retina. *Vision Res.* **26**, 223–238.

Marc, R.E. 1989 The anatomy of multiple GABAergic and glycinergic pathways in the inner plexiform layer of the goldfish retina. In *Neurobiology of the inner retina* (ed. R. Weiler & N. Osborne), pp. 53–64. Berlin: Springer-Verlag.

Marc, R.E. & Sperling, H.G. 1976 The chromatic organization of the goldfish cone mosaic. *Vision Res.* **16**, 1211–1224.

Mariani, A.P. 1990 Amacrine cells of the rhesus monkey retina. *J. comp. Neurol.* **301**, 382–400.

Masland, R.H. 1988 Amacrine cells. *Trends Neurosci.* **11**, 405–410.

Masland, R.H., Mills, J.W. & Cassidy, C. 1984 The functions of acetylcholine in the rabbit retina. *Proc. R. Soc. Lond.* B **223**, 121–139.

Naka, K.I. 1980 A class of catfish amacrine cells respond preferentially to objects which move vertically. *Vision Res.* **20**, 961–965.

Osborne, N.N. 1984 Indoleamines in the eye with special reference to serotonergic neurones of the retina. *Prog. Retinal Res.* **3**, 61–104.

Pourcho, R.G. 1980 Uptake of ^{3}H-glycine and ^{3}H-GABA by amacrine cells in the cat retina. *Brain Res.* **198**, 333–346.

Pourcho, R.G. & Goebel, D.J. 1983 Neuronal subpopulations in cat retina which accumulate the GABA agonist, ^{3}H-muscimol: a combined Golgi and autoradiographic study. *J. comp. Neurol.* **219**, 25–35.

Pourcho, R.G. & Goebel, D.J. 1988 Colocalization of substance P and gamma-aminobutyric acid in amacrine cells of the cat retina. *Brain Res.* **447**, 164–168.

Pourcho, R.G. & Owczarzak, M.T. 1991 Connectivity of glycine immunoreactive amacrine cells in the cat retina. *J. comp. Neurol.* **307**, 549–561.

Provencio, I., Loew, E.R. & Foster, R.G. 1992 Vitamin A_2-based visual pigments in fully terestrial vertebrates. *Vision Res.* **32**, 2201–2208.

Ramon y Cajal, S. 1933 *The structure of the retina* (compiled and translated by S. A. Thorpe & M. Glickstein). Springfield, Illinois: Charles C. Thomas, Co., 1972.

Sherry, D.M., Micich, A. & Yazulla, S. 1993 Glycine in the lizard retina: comparison to the GABA system. *Visual Neurosci.* **10**, 693–702.

Sherry, D.M. & Ulshafer, R.J. 1992*a* Neurotransmitter-specific identification and characterization of neurons in the all-cone retina of *Anolis carolinensis*. I. Gamma-aminobutyric acid. *Visual Neurosci.* **8**, 515–529.

Sherry, D.M. & Ulshafer, R.J. 1992*b* Neurotransmitter-specific identification and characterization of neurons in the all-cone retina of *Anolis carolinensis*. II. Glutamate and aspartate. *Visual Neurosci.* **9**, 313–323.

Sherry, D.M. & Yazulla, S. 1993*a* Goldfish bipolar cells and axon terminal patterns: a Golgi study. *J. comp. Neurol.* **329**, 188–200.

Sherry, D.M. & Yazulla, S. 1993*b* Immunofluorescent identification of endogenous neurotransmitter content in Golgi-impregnated neurons. *J. Neurosci. Meth.* **46**, 41–48.

Steinberg, R.H., Reid, M. & Lacy, P.L. 1973 The distribution of rods and cones in the retina of the cat (*Felis domesticus*). *J. comp. Neurol.* **148**, 229–248.

Stell, W.K., Ishida, A.T., & Lightfoot, D.O. 1977 Structural basis for On- and Off-center responses in retinal bipolar cells. *Science, Wash.* **198**, 1269–1271.

Stone, J. 1965 A quantitative analysis of the distribution of ganglion cells in the cat's retina *J. comp. Neurol.* **124**, 337–352.

Strettoi, E., Raviola, E. & Dacheux, R. 1990 Synaptic connections of the narrow-field, bistratified rod amacrine cell (AII) in the rabbit retina. *J. comp. Neurol.* **325**, 152–168.

Strettoi, E., Raviola, E. & Dacheux, R. 1992 Synaptic connections of rod bipolar cells in the inner plexiform layer of the rabbit retina. *J. comp. Neurol.* **295**, 449–466.

Studholme, K.M., Yazulla, S. & Phillips, C.J. 1987 Interspecific comparisons of immunohistochemical localization of retinal neurotransmitters in four species of bats. *Brain. Behav. Evol.* **30**, 160–173.

Su, Y.Y.T., Wu, J.-Y. & Lam, D.M.K. 1979 Purification of L-glutamic acid decarboxylase from catfish brain. *J. Neurochem.* **33**, 169–179.

Teranishi, T., Negishi, K. & Kato, S. 1987 Functional and morphological correlates of amacrine cells in carp retina. *Neuroscience* **29**, 935–950.

Teranishi, T. & Negishi, K. 1991 Dendritic morphology of a class of interstitial and normally placed amacrine cells revealed by intracellular Lucifer Yellow injection in carp retina. *Vision Res.* **31**, 463–475.

Underwood, G. 1951 Reptilian retinas. *Nature, Lond.* **167**, 183–185.

Vallerga, S. 1981 Physiological and morphological identification of amacrine cells in the retina of the larval tiger salamander. *Vision Res.* **21**, 1307–1313.

Wagner, H.J. & Wagner, E. 1988 Amacrine cells of a teleost fish, the roach (*Rutilus rutilis*): a Golgi study on differentiation and layering. *Phil. Trans. R. Soc. Lond.* B **321**, 263–324.

Wässle, H. & Boycott, B.B. 1991 Functional architecture of the mammalian retina. *Physiol. Rev.* **72**, 447–480.

Wässle, H. & Chun, M.H. 1988 Dopaminergic and indoleamine-accumulating amacrine cells express GABA-like immunoreactivity in the cat retina. *J. Neurosci.* **8**, 3383–3394.

Watt, C.B. 1992 A double-label study demonstrating that all serotonin-like immunoreactive amacrine cells in the larval tiger salamander retina express GABA-like immunoreactivity. *Brain Res.* **583**, 336–339.

Weiler, R. & Ball, A.K. 1984 Co-localization of neurotensin-like immunoreactivity and ^{3}H-glycine uptake system in sustained amacrine cells of turtle retina. *Nature, Lond.* **311**, 759–761.

Weiler, R. & Schütte, M. 1985 Kainic acid-induced release of serotonin from OFF-bipolar cells in the turtle retina. *Brain Res.* **360**, 379–383.

Wenthold, R., Zemple, J., Parakkal, M.A., Reeks, K.A. & Altschuler, R.A. 1986 Immunocytochemical localization of GABA in the cochlear nucleus of the guinea pig. *Brain Res.* **380**, 7–18.

Wenthold, R.J., Huie, D., Altschuler, R.A. & Reeks, K.A. 1987 Glycine immunoreactivity localized in the cochlear nucleus and superior olivary complex. *Neurosci.* **22**, 897–912.

West, R.W. 1972 Superficial warming of epoxy blocks for cutting of 25–150 μm sections to be resectioned in the 40–90 μm range. *Stain Technol.* **47**, 201–204.

Witkovsky, P., Eldred, W. & Karten, H.J. 1984 Catecholamine- and indoleamine-containing neurons in the turtle retina. *J. comp. Neurol.* **228**, 217–225.

Wulle, I. & Wagner, H.-J. 1990 GABA and tyrosine hydroxylase immunocytochemistry reveal different patterns of colocalization in retinal neurons of various vertebrates. *J. comp. Neurol.* **296**, 173–178.

Yang, C.-Y., Lukasiewicz, P., Maguire, G., Werblin, F.S. & Yazulla, S. 1991 Amacrine cells in the tiger salamander retina: Morphology, physiology, and neurotransmitter identification. *J. comp. Neurol.* **312**, 19–32.

Yazulla, S. 1986 GABAergic mechanisms in the retina. *Prog. Retinal Res.* **5**, 1–52.

Yazulla, S. 1991 The mismatch problem for GABAergic amacrine cells in goldfish retina: resolution and other issues. *Neurochem. Res.* **16**, 327–339.

Yazulla, S. & Studholme, K.M. 1990 Multiple subtypes of glycine-immunoreactive neurons in the goldfish retina: single- and double-label studies. *Visual Neurosci.* **4**, 299–309.

Yazulla, S. & Yang, C.-Y. 1988 Colocalization of GABA- and glycine-immunoreactivities in a subset of retinal neurons in tiger salamander. *Neurosci. Lett.* **95**, 37–41.

Received 8 February 1993; accepted 8 March 1993

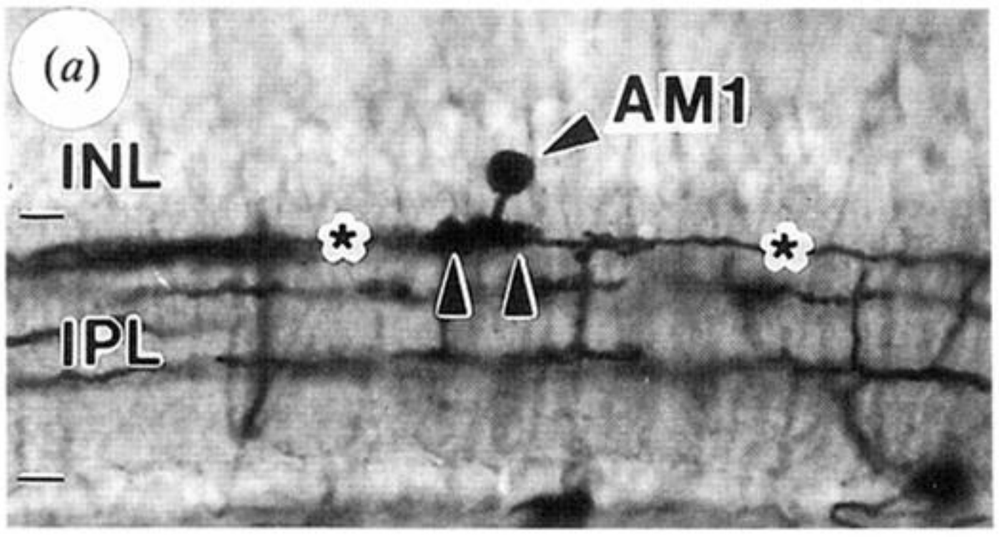

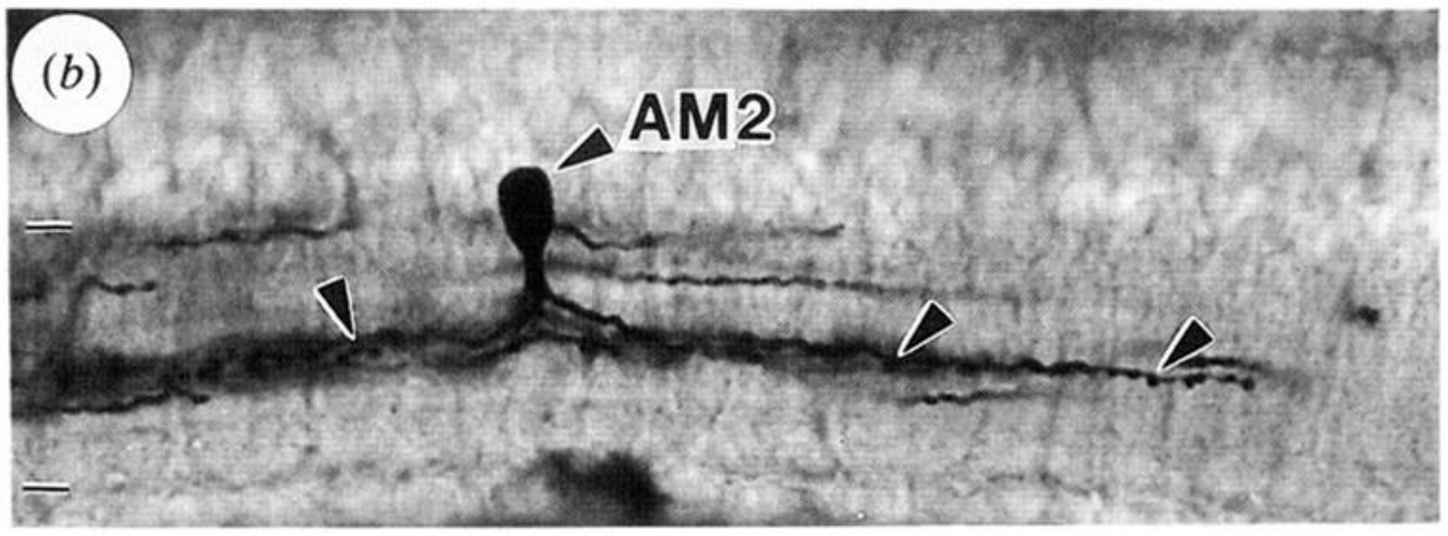

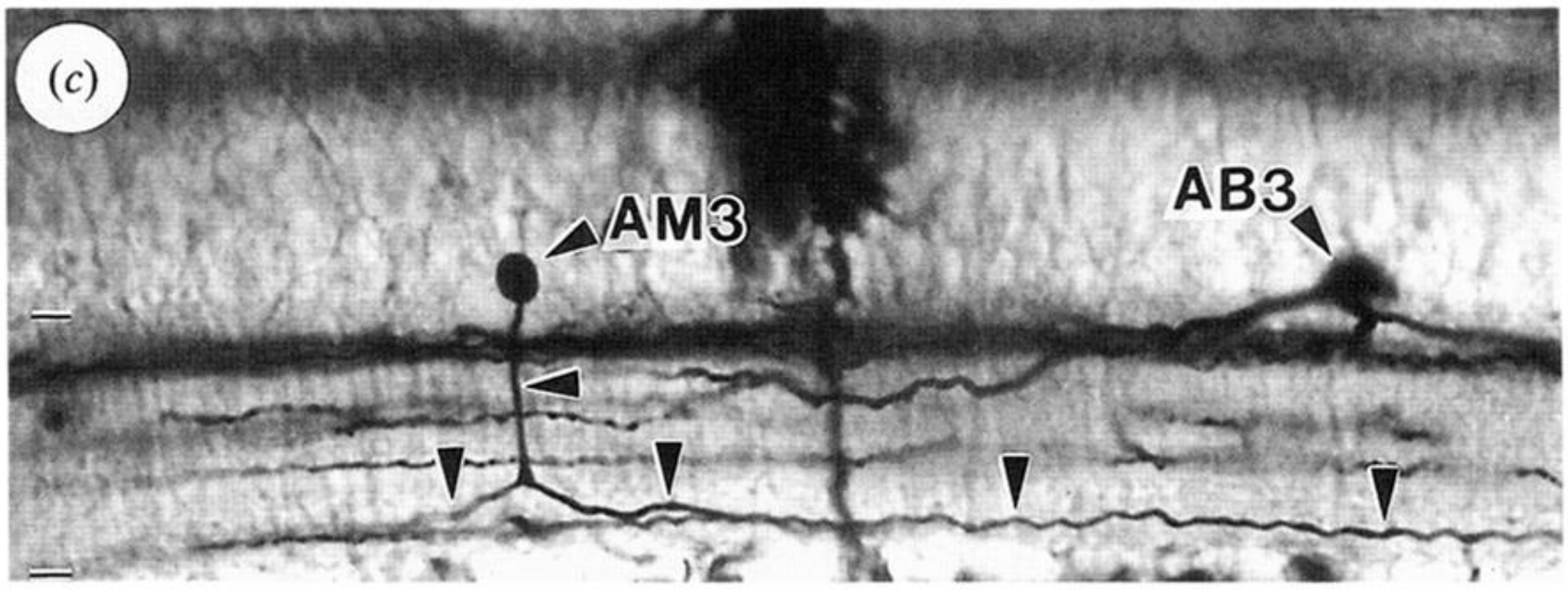

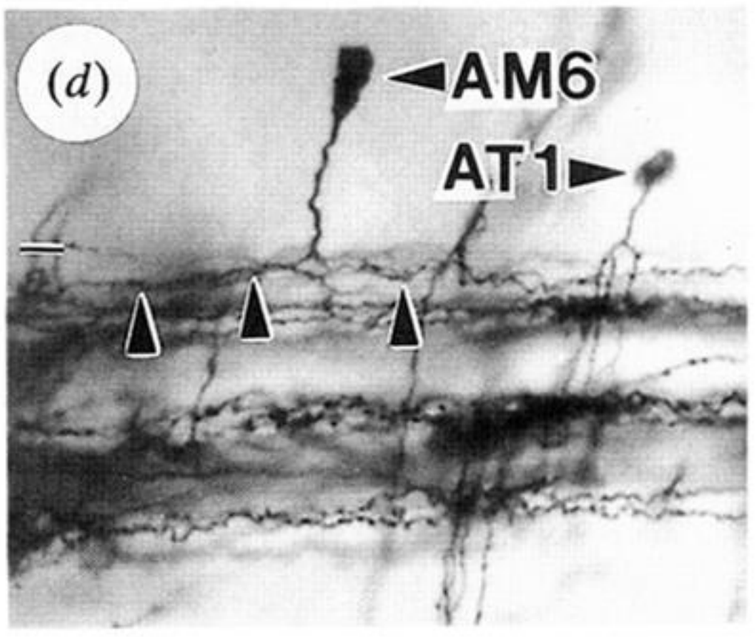

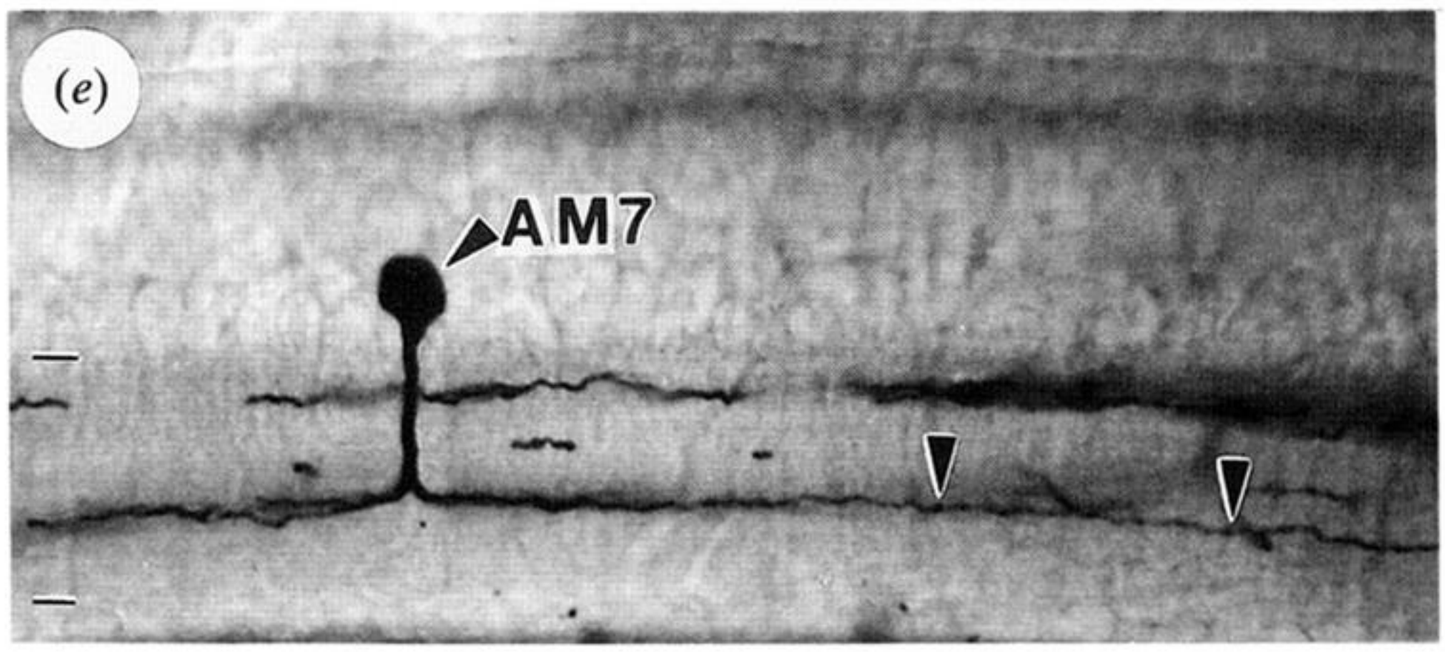

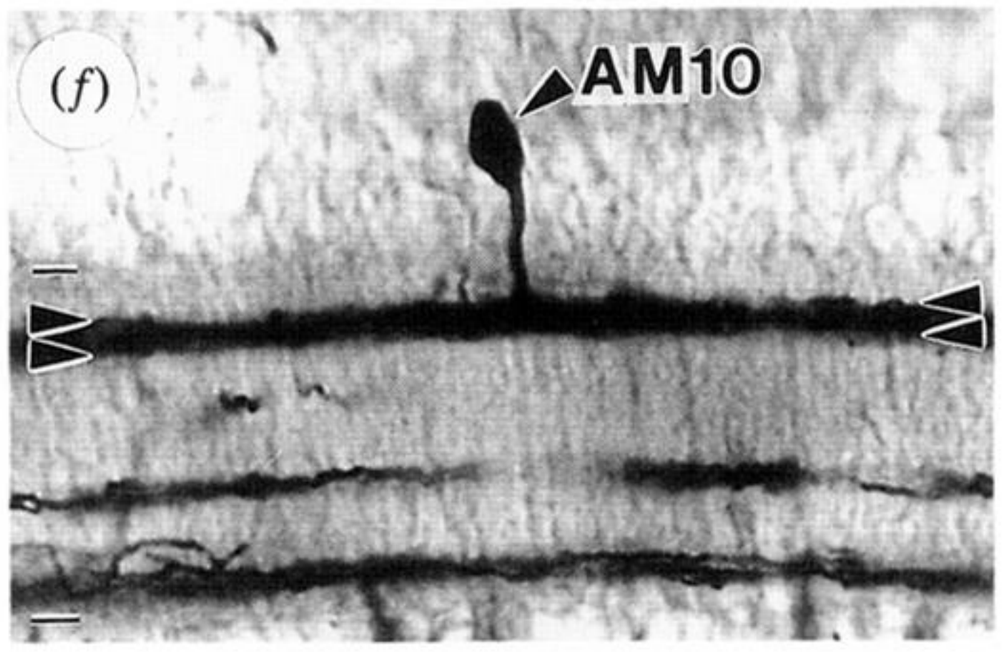

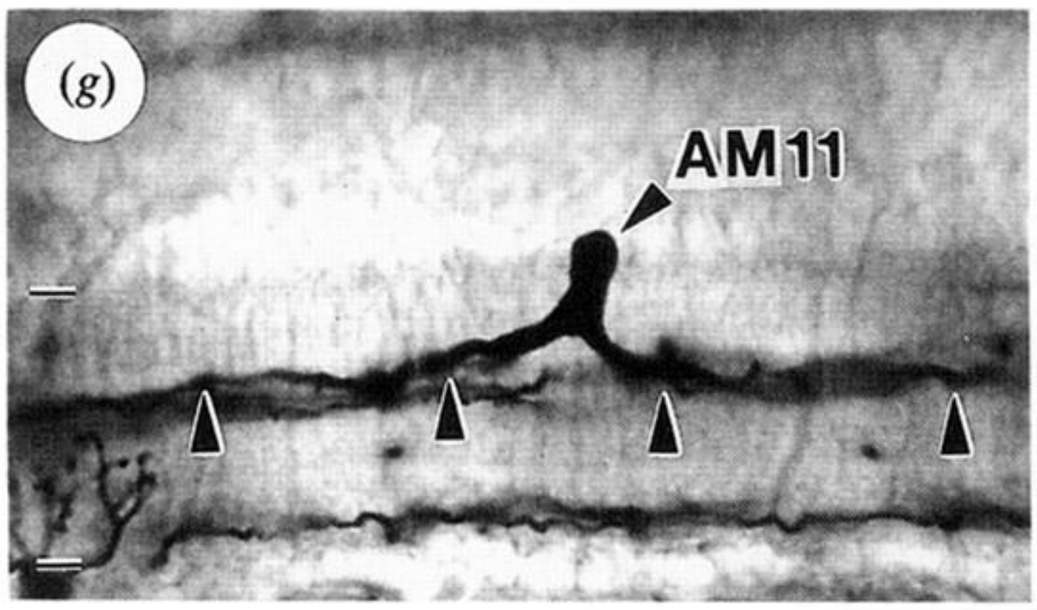

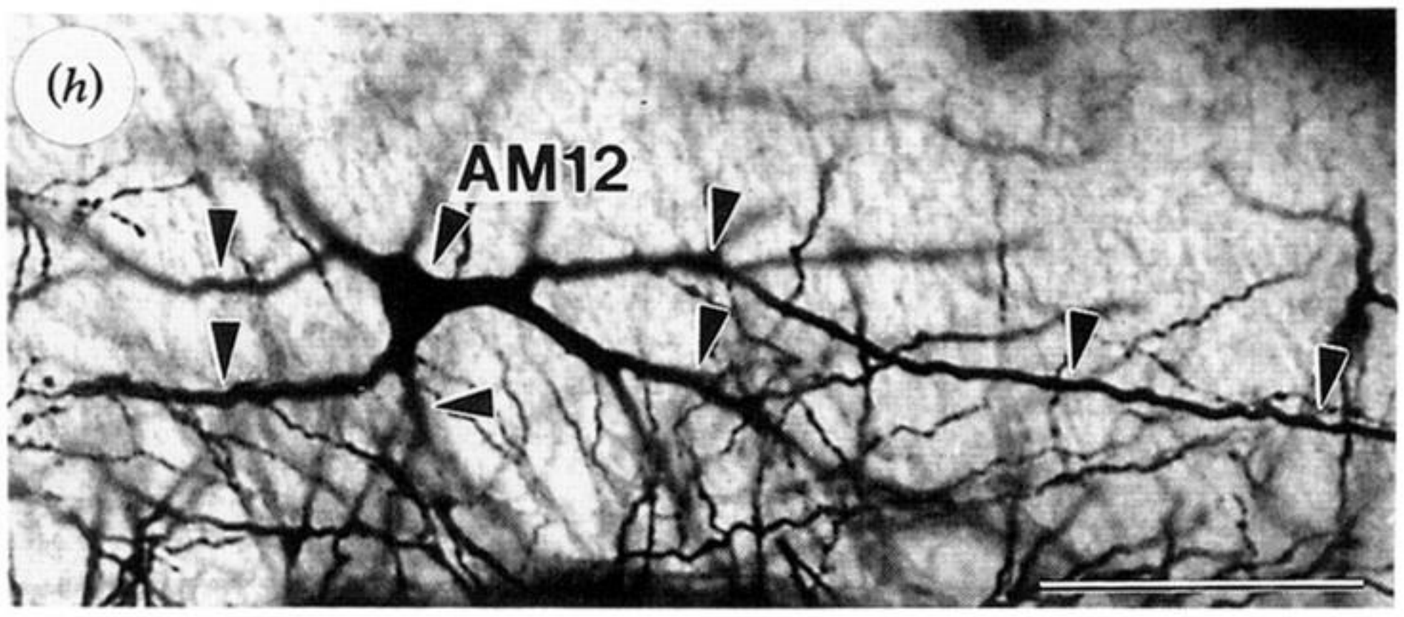

Figure 1. Golgi impregnated monostratified amacrine cells. Tick marks show the borders of the IPL. (*a*) AM1 cell with its characteristic cloud of boutons (arrowheads). Golgi-stained processes from other cells (asterisks) pass through the boutons. (*b*) AM2 cell with its bouton-bearing dendrites ramifying in the mid IPL (arrowheads). (*c*) AM3 cell of the AM3.2 subtype with a relatively thick primary dendrite and secondary dendrites coursing in opposite directions deep within the IPL (arrowheads). A bistratified AB3 cell is also present. (*d*) AM6 cell with its distally placed, rhomboidal soma. This cell gives rise to several fine dendrites in the distal IPL (arrowheads). A Golgi-stained AT1 cell also is present. (*e*) AM7 cell of the AM7.2 subtype. These cells are characterized by a pyriform soma, a relatively thick descending dendrite and few secondary dendrites with boutons (arrowheads). (*f*) AM10 cell of the AM10.1 subtype, with a distally placed soma, thick descending dendrite and dense plexus of secondary dendrites in the distal IPL (arrowheads). (*g*) AM11 cell with the characteristic cylindrical soma and stout, sparsely branched dendrites (arrowheads). (*h*) AM12 interstitial amacrine cell seen in tangential section. The soma is contained within the depth of the IPL and gives rise to several stout, sparsely branched dendrites (arrowheads). Calibration bar = 50 μm for all micrographs.

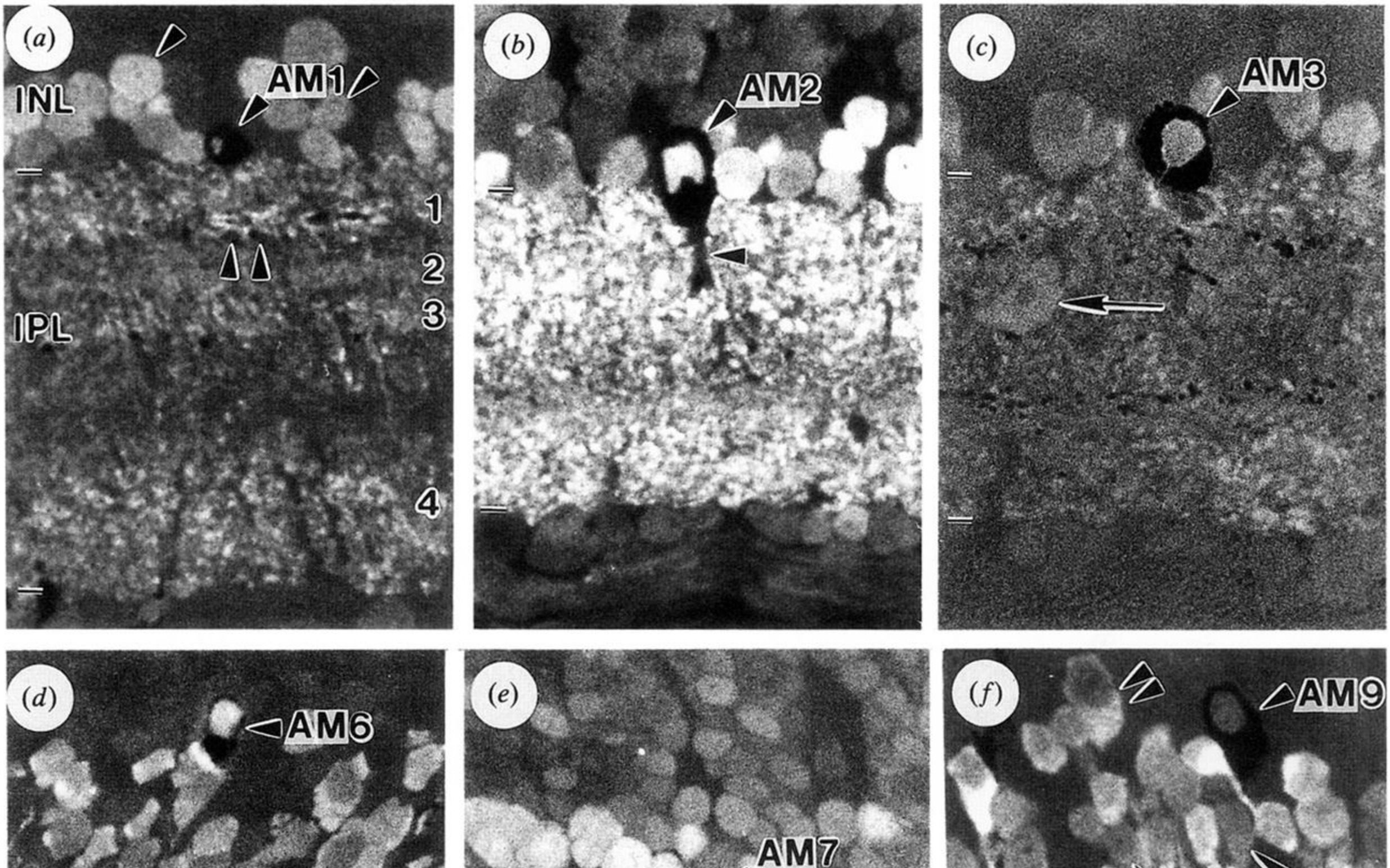

Figure 4. Combined bright field-fluorescence micrographs of several GABA-IR monostratified amacrine cell types. (*a*) GABA-IR in the nucleus of a Golgi impregnated AM1 cell. Single arrowheads show other non-impregnated GABA-IR amacrine cells. Double arrowheads in the IPL show some boutons from the AM1 cell's dendrites. GABA-IR in the IPL shows the typical four layered pattern (1–4). (*b*) Intense GABA-IR in an AM2 cell. The descending dendrite of the cell is also visible (arrowhead). (*c*) Double-labelled AM3 cell of the AM3.1 cell type. A non-impregnated GABA-IR interstitial cell is visible in the IPL (arrow). Note, the Golgi deposits in the distal IPL are not from the AM3.1 cell shown. (*d*) A double-labelled AM6 cell. Note the distal placement of the soma. (*e*) An example of a GABA-IR AM7.3 cell. Part of the cell's descending process is visible in the IPL (arrowheads). (*f*) GABA-IR in the nuclei of AM9 cells is typically weak, but computer-assisted thresholding shows these GABA-IR levels to be above background and similar in intensity to other weakly GABA-IR cells (arrows). A non-impregnated cell similar in appearance to the AM9 cell that shows strong somatic GABA-IR and weak nuclear GABA-IR is also visible (double arrowheads). Calibration bar = 20 μm.

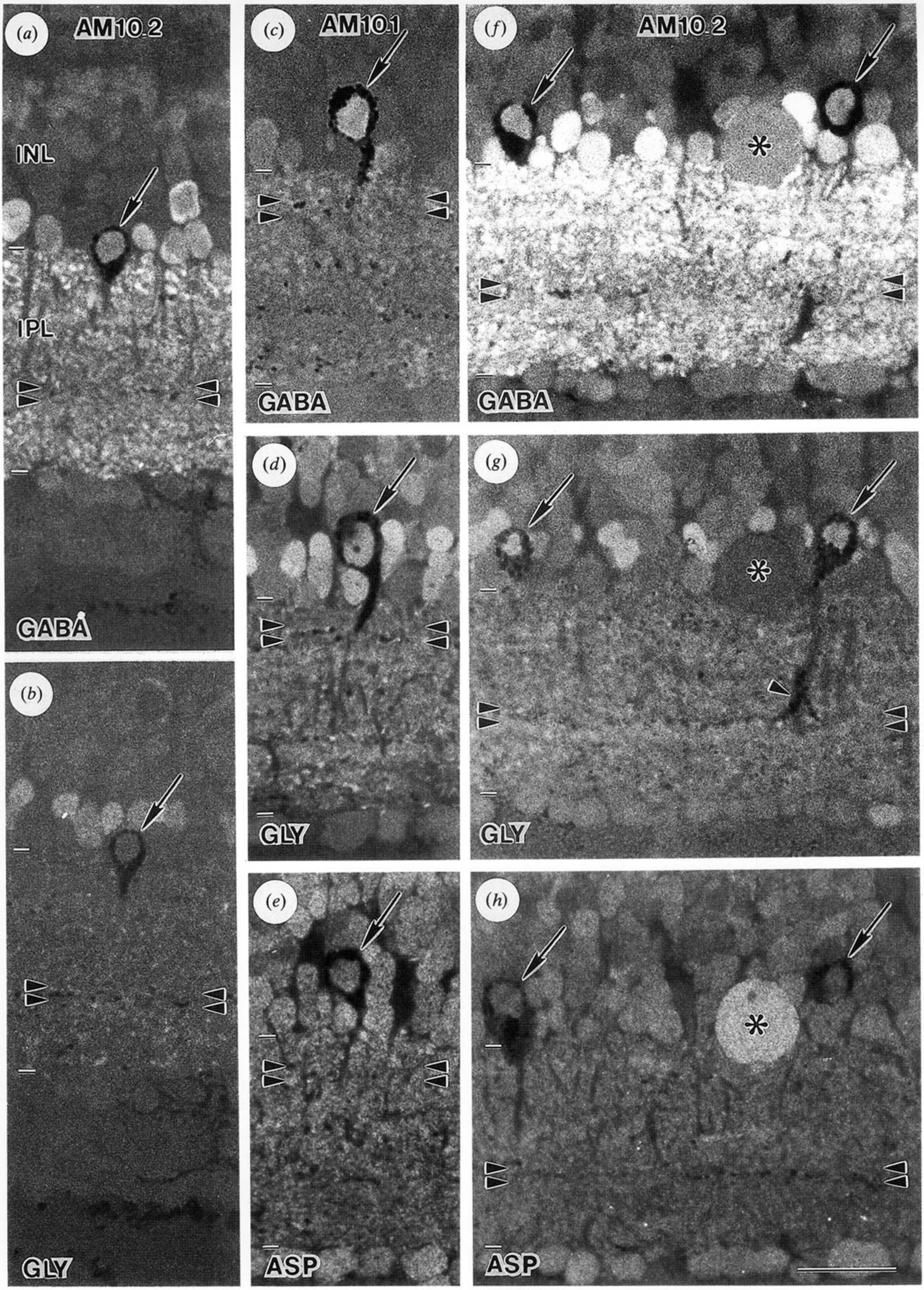

Figure 6. Neurochemical heterogeneity in AM10 cells demonstrated by postembedding immunocytochemistry on serial sections of Golgi-stained cells. Arrowheads in all micrographs show the ramification level of the Golgi-stained cells. (*a*,*b*) Serial sections of an AM10.2 cell (arrow) that contains GABA-IR (*a*), but not GLY-IR (*b*). (*c*–*e*) Serial sections of a Golgi-stained AM10.1 cell (arrow) reacted for GABA-IR (*c*), GLY-IR (*d*) and ASP-IR (*e*). The cell shows both GABA-IR and GLY-IR, but not ASP-IR. (*f*–*h*) Serial sections of two AM10.2 amacrine cells (arrows) reacted for GABA-IR (*f*), GLY-IR (*g*) and ASP-IR (*h*). A large spherical cell (asterisk) is present in all three micrographs and shows weak GABA-IR, no GLY-IR and strong ASP-IR, typical of this cell type (Sherry & Ulshafer 1992*b*). Calibration bar = 20 μm.

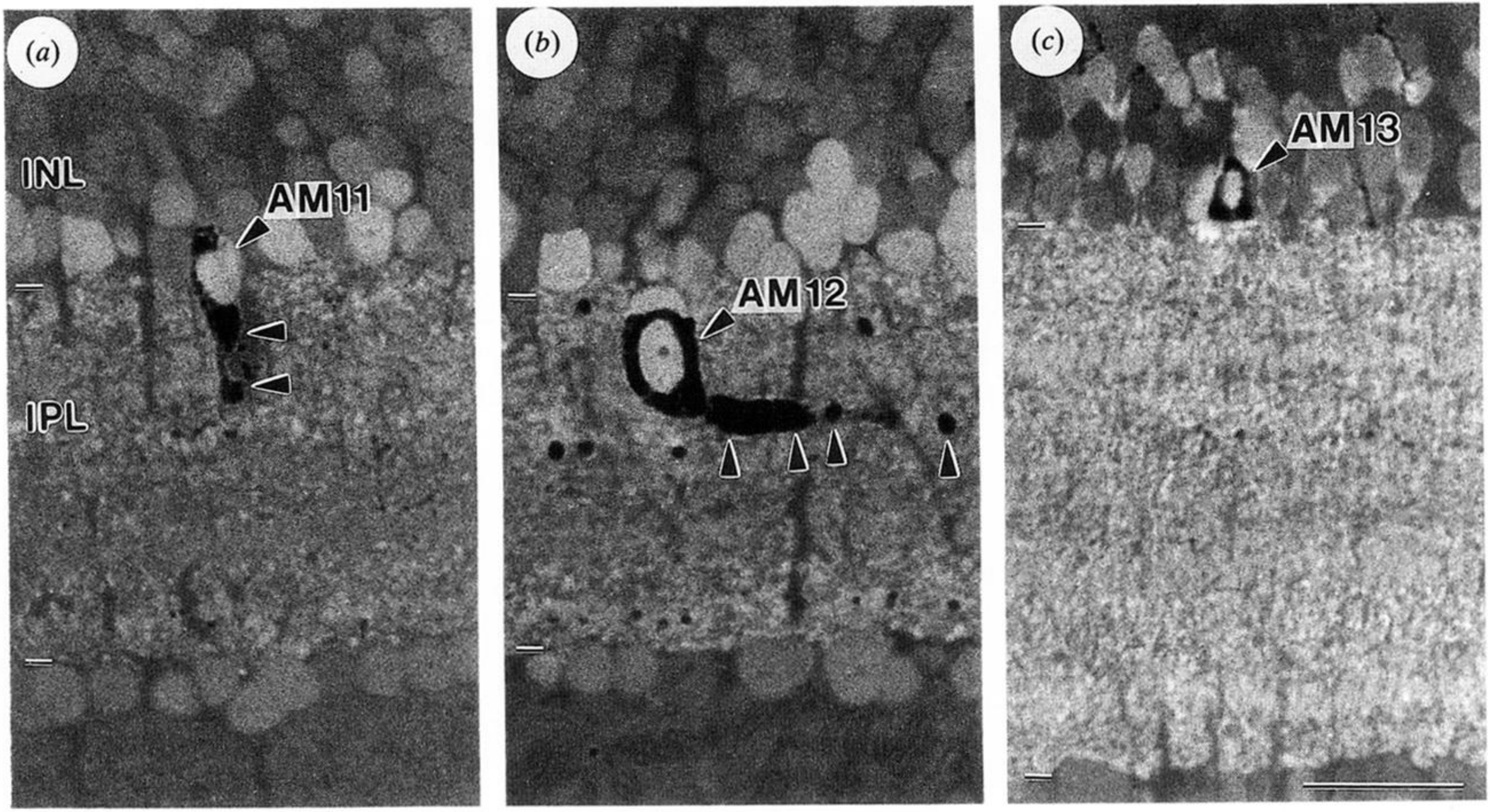

Figure 8. GABA-IR in AM11, AM12 and AM13 cells. (*a*) AM11 cell with an eccentrically placed, GABA-IR nucleus. Part of the descending process of this cell also is visible (arrowheads). (*b*) AM12 interstitial amacrine cell in the IPL. One of the cell's stout primary dendrites is present (arrowheads). (*c*) Example of a GABA-IR AM13 cell. Calibration bar = 20 μm.

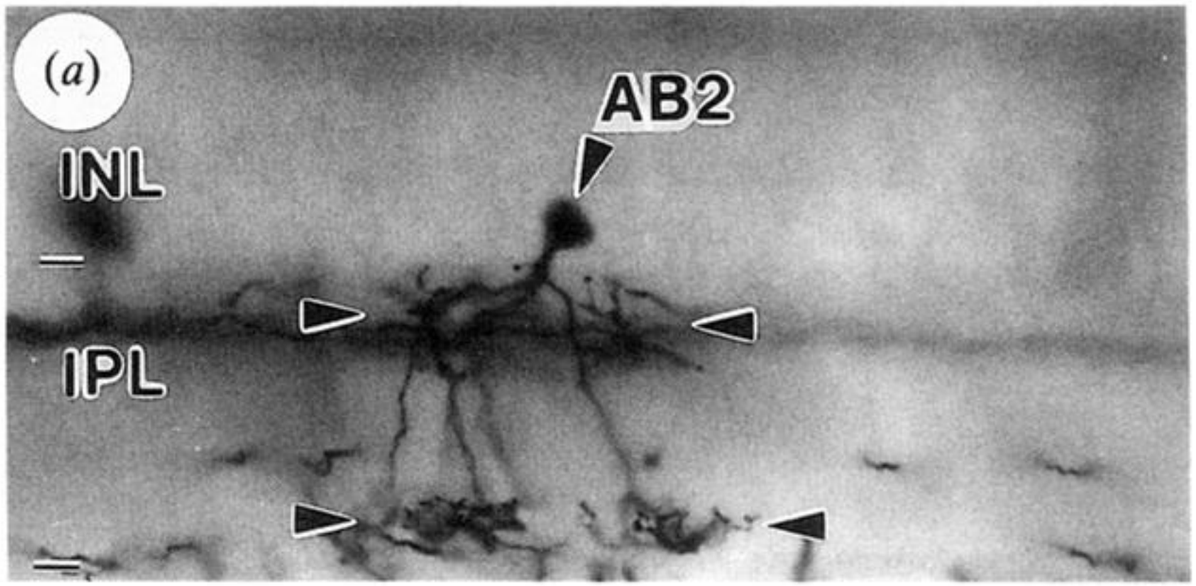

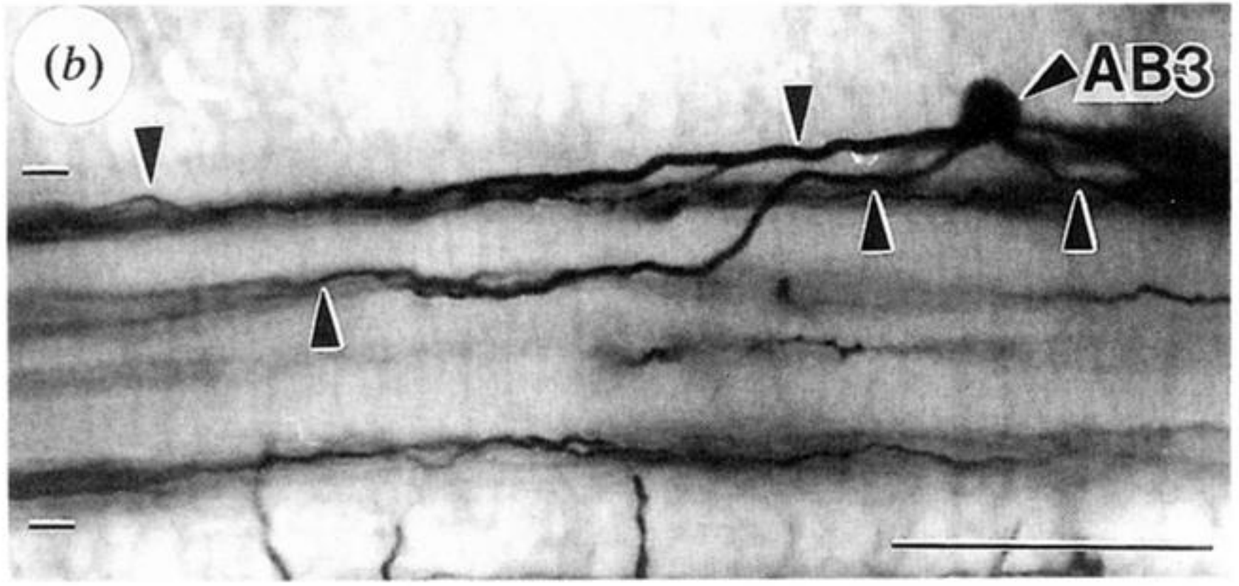

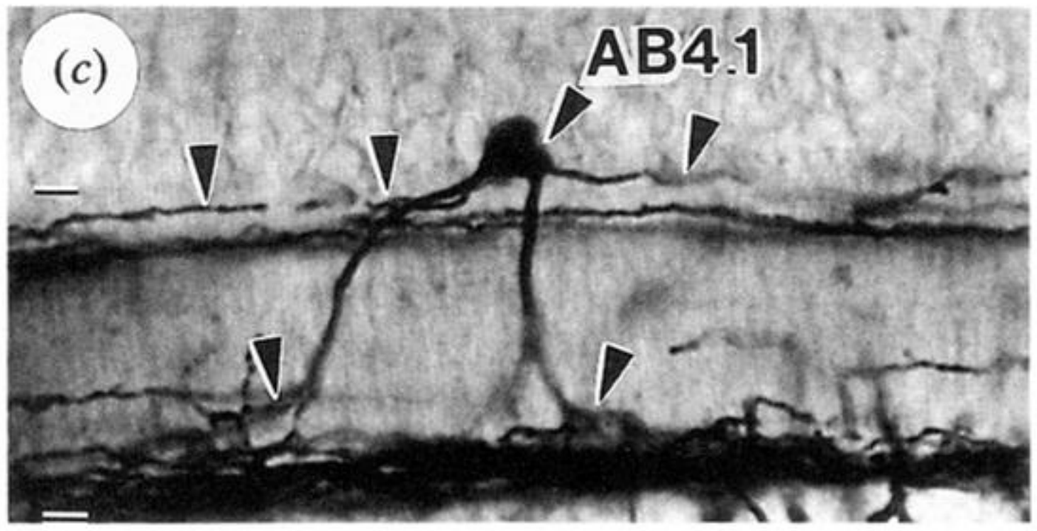

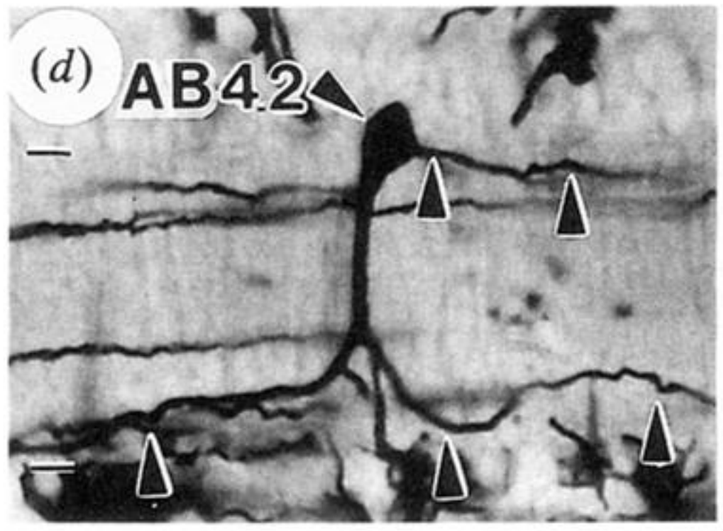

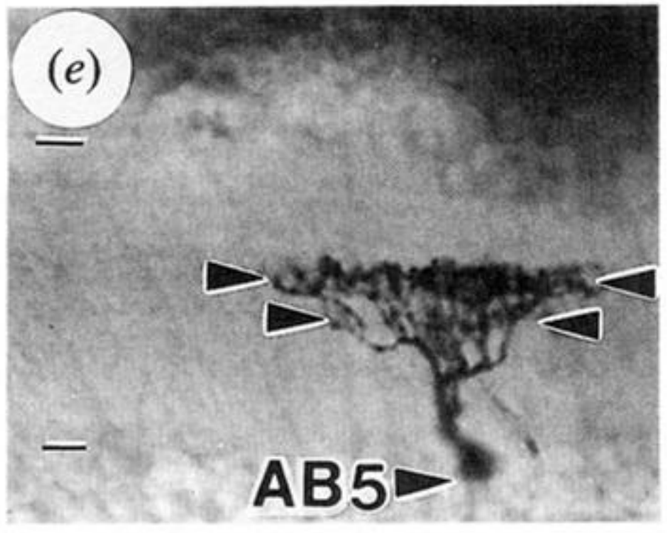

Figure 9. Golgi-stained bistratified amacrine cells. (*a*) AB2 cell with somewhat diffuse arborizations in the distal and proximal IPL (arrowheads). (*b*) AB3 cell stratifying in the distal and mid IPL (arrowheads). (*c*) AB4.1 amacrine cell with a multipolar soma and dendritic stratifications in the distal and proximal IPL (arrowheads). (*d*) AB4.2 cell. These cells are distinguished from AB4.1 cells by their pyriform soma, a single stout process descending to the proximal IPL, and a single process coursing in the distal IPL (all processes shown by arrowheads). Golgi-stained processes not marked with arrowheads arise from other impregnated cells nearby. (*e*) A displaced AB5 amacrine cell with a distinct stratum of boutons in the mid IPL and a smaller stratum of boutons at a more proximal depth in the IPL (arrowheads). Calibration bar = 50 μm.

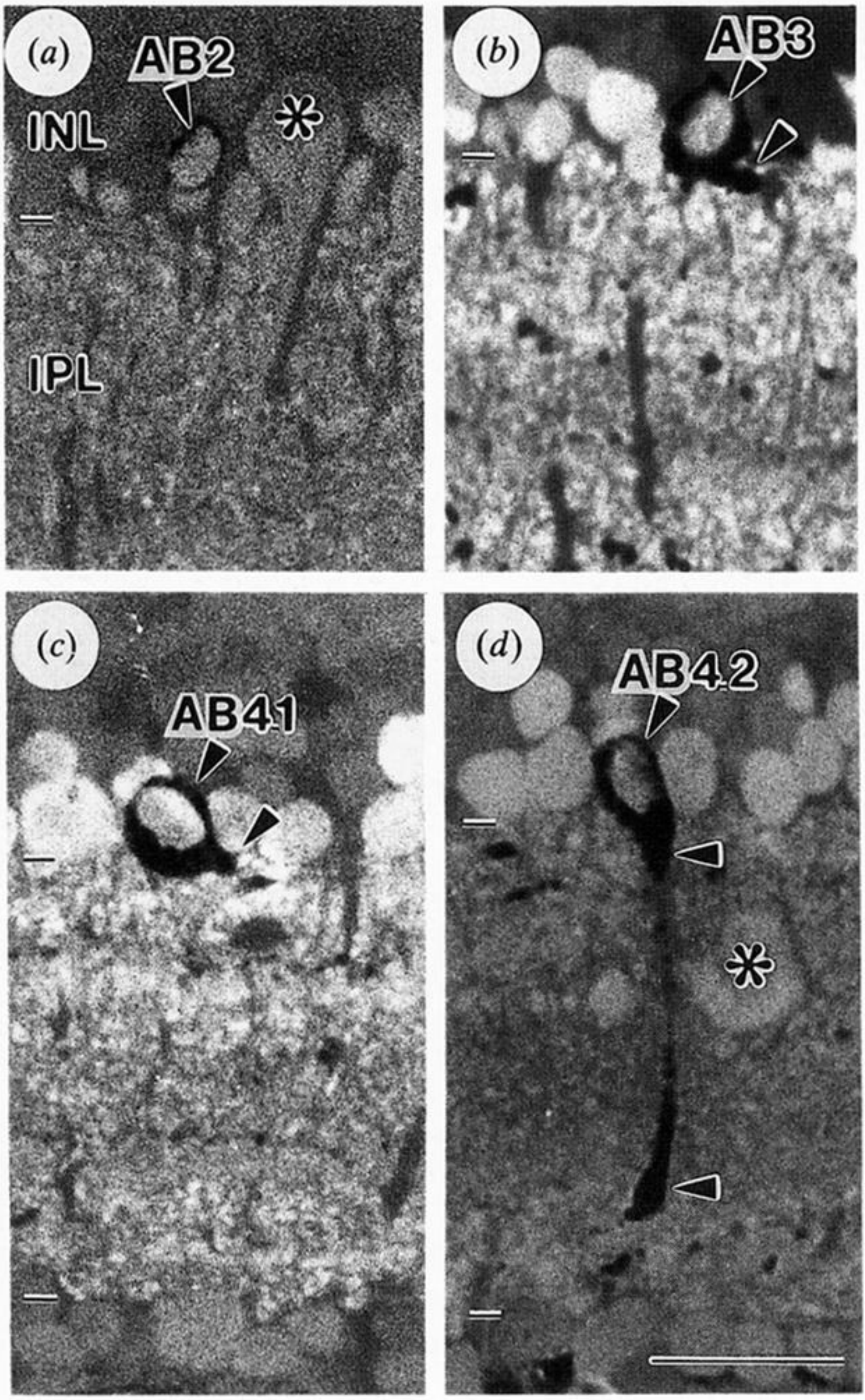

Figure 11. GABA-IR in Golgi-stained bistratified amacrine cells. (*a*) AB2 cell showing GABA-IR. A prominent non-impregnated amacrine cell showing GABA-IR (asterisk) is located nearby. (*b*) Intense GABA-IR in an AB3 cell. One of the primary dendrites can be seen leaving the soma (arrowhead). (*c*) Example of a GABA-IR AB4.1 cell showing a portion of one of the primary dendrites (arrowhead). (*d*) AB4.2 cell showing GABA-IR. The descending process of the cell is visible (arrowheads) and a non-impregnated, GABA-IR interstitial amacrine cell (asterisk) also is visible in the IPL. Calibration bar = 20 μm.

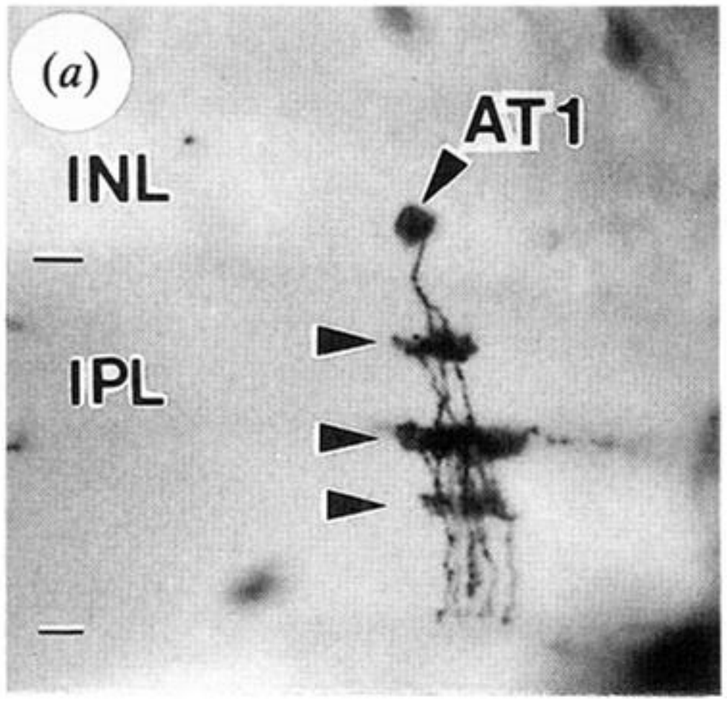

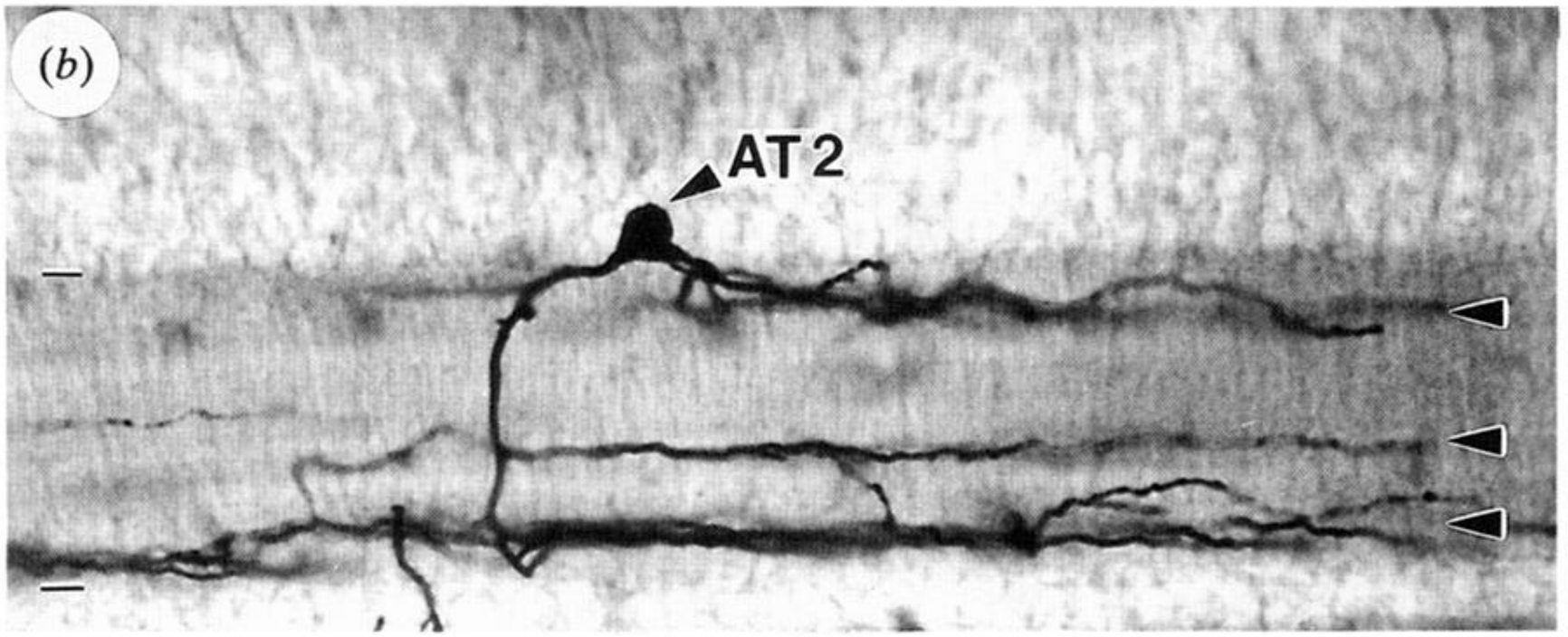

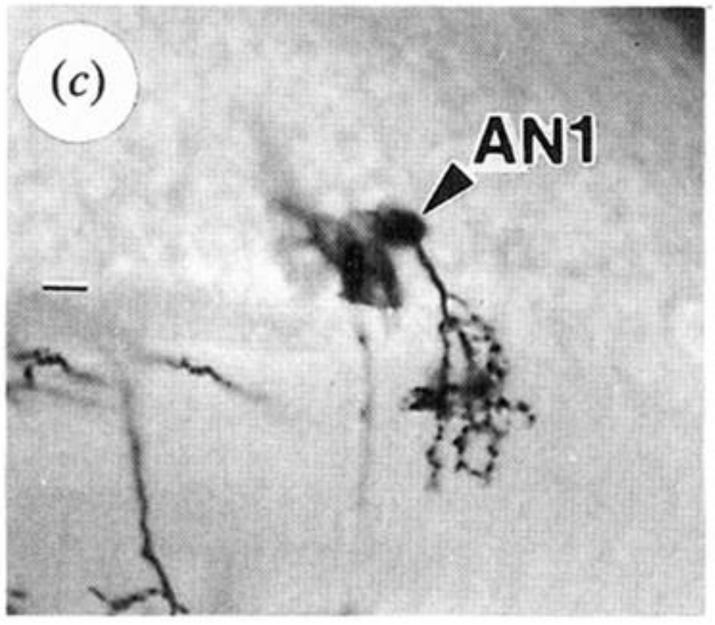

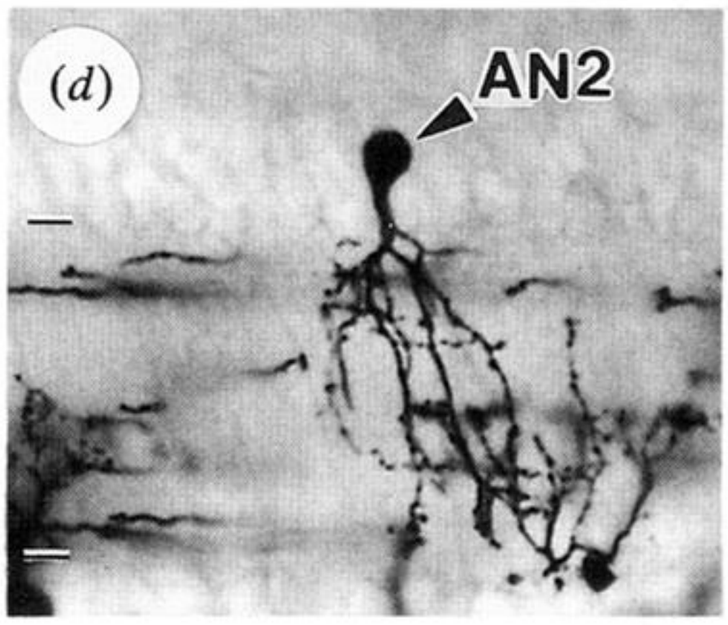

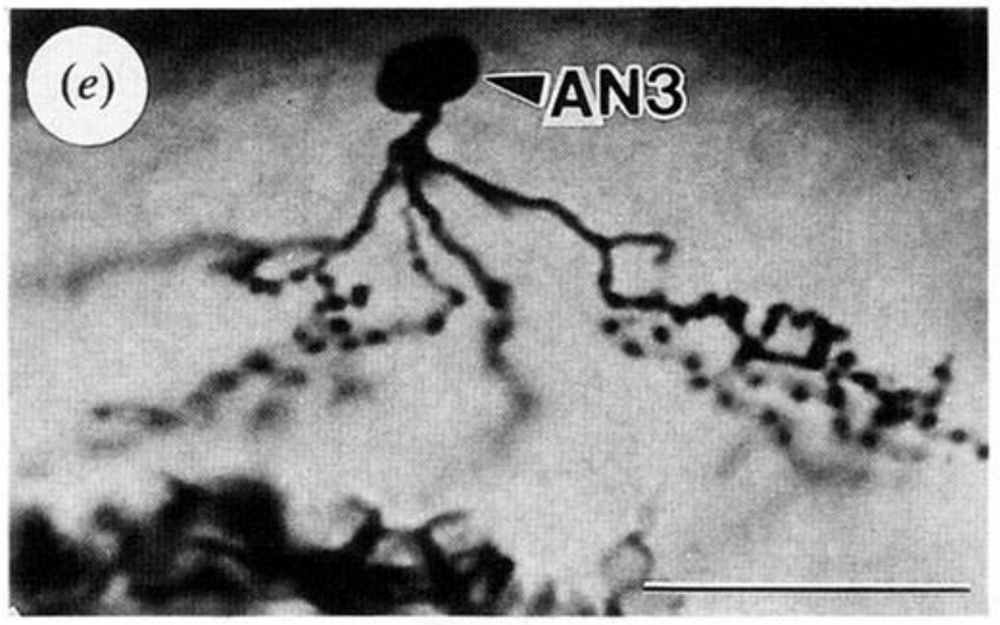

Figure 12. Golgi-stained tristratified and non-stratified cells. (*a*) A very narrow field 'Medusa' AT1 cell. The three tiers of boutons are clearly visible (arrowheads). (*b*) A multipolar tristratified AT2 cell. The three dendritic strata are shown with arrowheads. (*c*) Example of a very narrow field AN1 cell. The non-stratified dendrites of this cell type were restricted to the distal IPL and possessed many boutons. (*d*) A non-stratified AN2 cell with dendrites ramifying throughout the depth of the IPL. Processes from a Golgi-stained ganglion cell are visible in this micrograph, but close inspection showed no contact between the two cells. (*e*) Example of an AN3 amacrine cell characterized by large boutons along the dendrites and a narrow dendritic field in the distal IPL. Calibration bar = 50 μm.

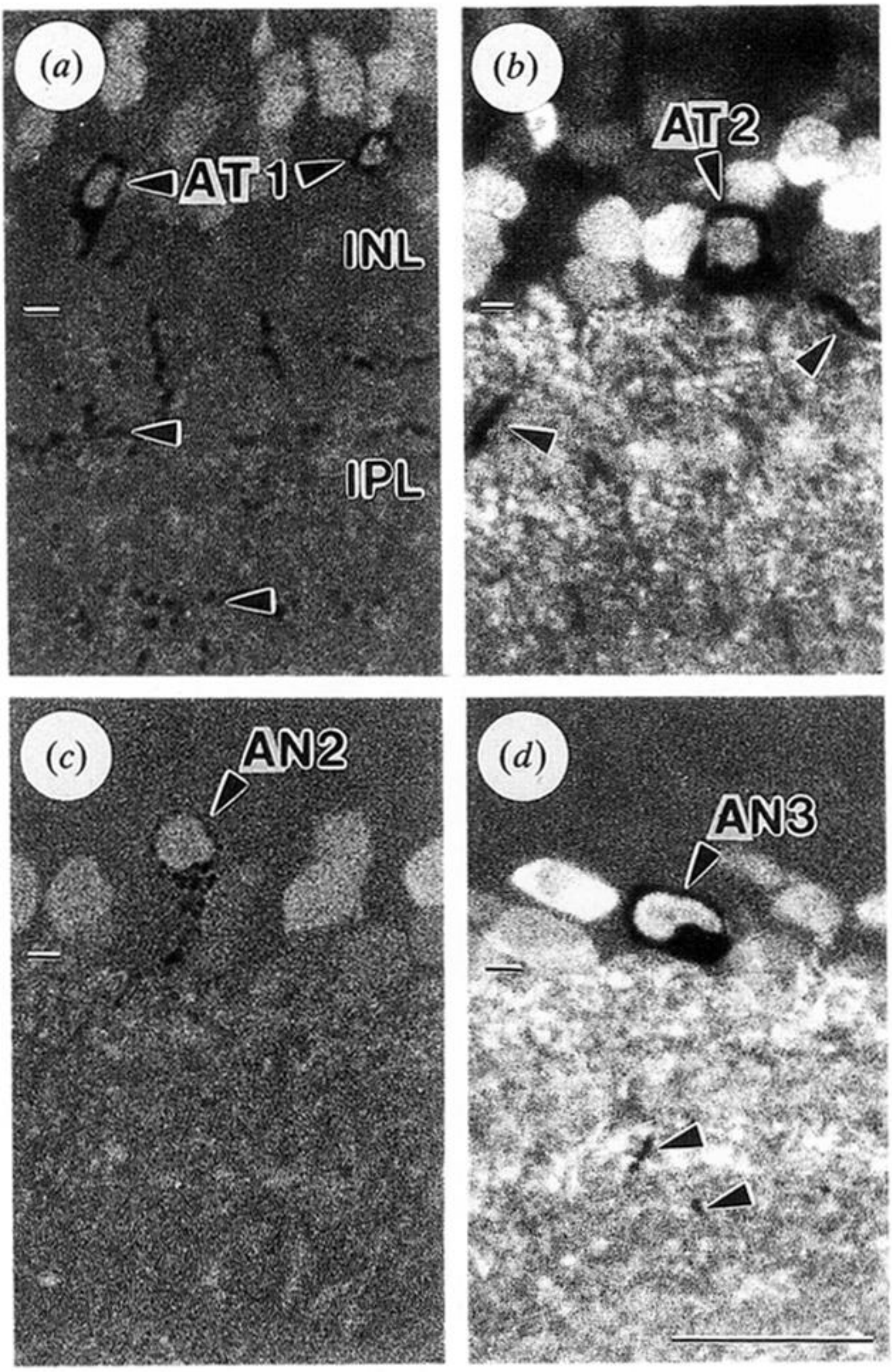

Figure 14. GLY-IR and GABA-IR in tristratified and non-stratified amacrine cells. (*a*) Two GLY-IR AT1 'Medusa' cells are present in the micrograph. Two tiers of boutons belonging to the cell on the left are visible in the IPL (arrowheads). (*b*) GABA-IR in the nucleus of the AT2 cell. Parts of the dendrites of this cell can be seen in the IPL (arrowheads). (*c*) GABA-IR in an AN2 cell. The Golgi deposits in this cell have a granular appearance. (*d*) Intense GABA-IR in an AN3 cell. Some boutons from this cell can be seen in the IPL (arrowheads). Calibration bar = 20 μm.

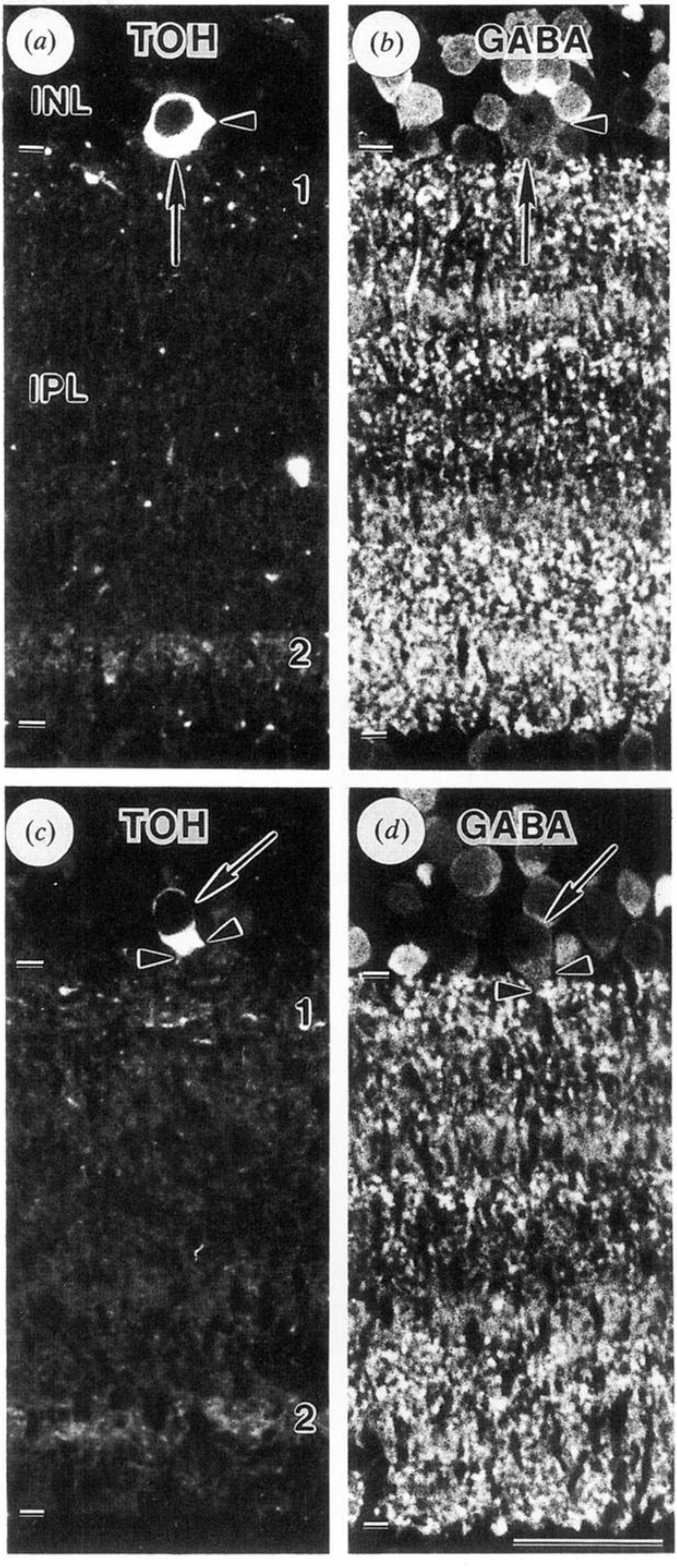

Figure 15. Serial section demonstration of TOH-IR and GABA-IR colocalization in AB4.1 (*a*,*b*) and AB4.2 (*c*,*d*) cells. (*a*,*b*) TOH-IR in an amacrine cell with AB4.1 characteristics (arrow in *a*). TOH-IR is present in two strata in the IPL (1,2) at depths similar to the stratification depth of AB4 cells. The same cell shows GABA-IR on a serial section (arrow in *b*). The arrowhead in both micrographs points to a protrusion on the cell body that may give rise to an ascending process. (*c*,*d*) TOH-IR in a pyriform amacrine cell with AB4.2 characteristics (arrow in *c*). Two protrusions that probably represent the origin of the primary dendrites are visible (arrowheads). Two TOH-IR strata are present in the IPL (1,2). The same cell seen in a serial section shows moderately intense GABA-IR (arrow in *d*). Calibration bar = 20 μm.

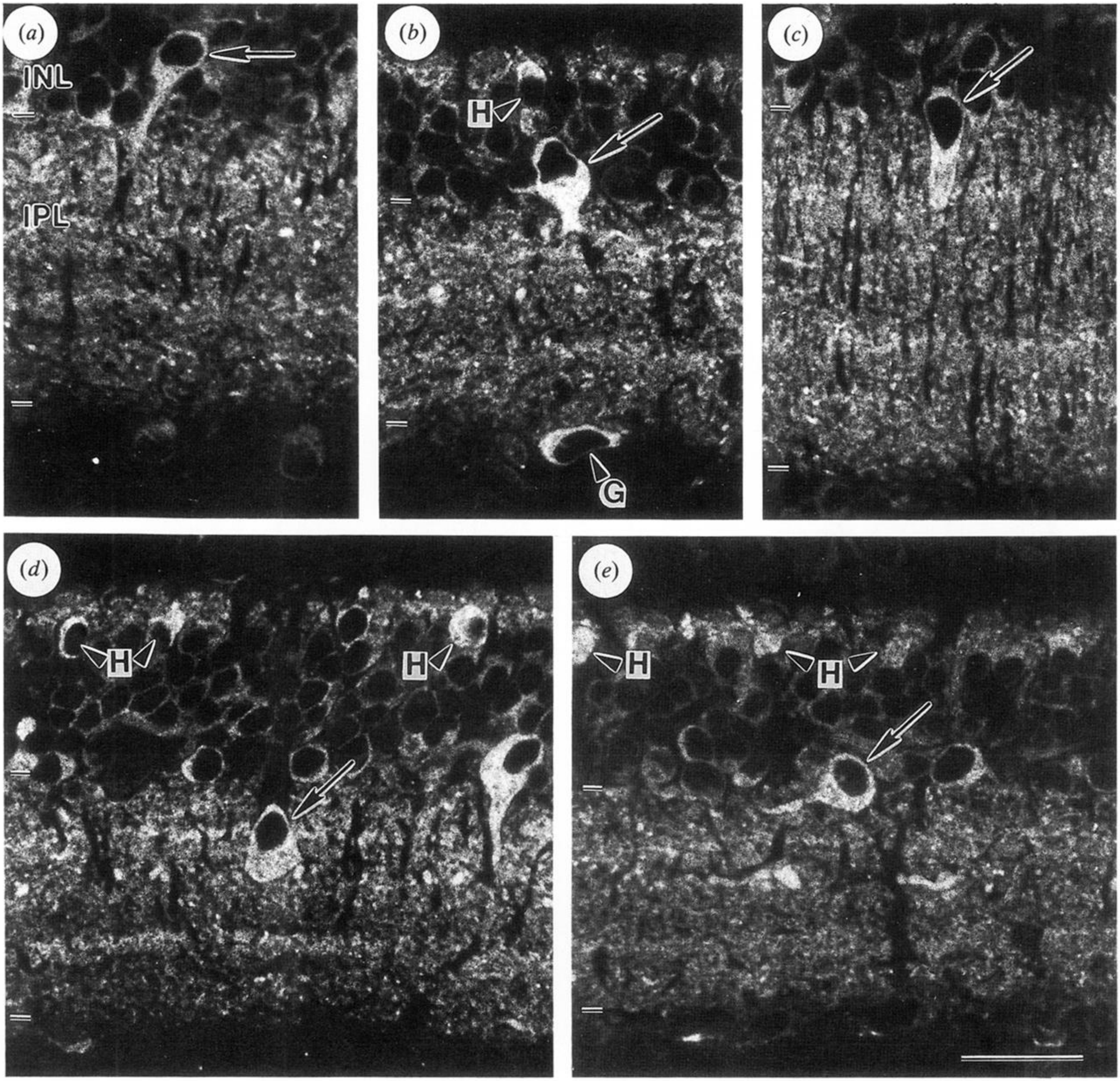

Figure 16. GAD-IR in the *Anolis* retina. GAD-IR is seen in horizontal and amacrine cells, cells in the ganglion cell layer and shows lamination in the IPL. (*a*) GAD-IR in a cell similar to an AM7 cell (arrow). (*b*) Intense GAD-IR in a large pyriform amacrine cell (arrow), similar in appearance to AM9 or AM10 cells. GAD-IR also is seen in a horizontal cell (H) and a cell in the ganglion cell layer (G). (*c*) GAD-IR in an amacrine cell (arrow) with the appearance of an AM11 cell. (*d*) GAD-IR in an interstitial amacrine (AM12) cell (arrow). Horizontal cells (H) and a large pyriform amacrine cell also show GAD-IR. (*e*) A multipolar amacrine cell showing GAD-IR (arrow) that could correspond to any of the AM13, AB3, AB4.1 or AT2 cell types. GAD-IR horizontal cells (H) and their processes also are present. Calibration bar = 20 μm.